Marine Turbulence

Lars Umlauf and Hans Burchard

June 26, 2020

Contents

Chapter 1

Phenomenology of turbulence

1.1 Coffee with milk?

Turbulence is a stochastic flow phenomenon that may occur in various fluids and gases. Turbulent flows have been observed on a broad range of spatial and temporal scales, ranging from rapidly changing, millimeter-scale engineering flows up to the slow, large-scale motions that govern the flow of giant gaseous planets (Jupiter is an example), and stars like the sun. Due to the many different faces of turbulence, its random character, and its kinematic complexity, a generally valid theory is lacking, and turbulence remains one of the major unsolved problems of classical physics. Nevertheless, a number special classes of turbulent flows have been described quite successfully with different types of modeling approaches. These notes provide a short introduction into the basic concepts with a focus on geophysical, and in particular oceanic flows.

Before we turn to the ocean, let us start with a thought experiment revealing one of the most important consequences of turbulence for the transport of matter, heat, and momentum: turbulent flows are generally associated with a drastic increase of mixing and transport rates compared to laminar flows. This is easily seen from a flow phenomenon that many of us observe every morning when we stir our cup of coffee. Our goal, after pouring milk into the coffee, clearly is to create a homogeneous mixture of milk and coffee. To this end, we could of course wait (without stirring) until molecular diffusion would have mixed milk and coffee — but experience shows that this would take hours or even days, and the coffee would be cold rather than mixed before the milk is evenly distributed.

We know, however, from the Fickian law that the diffusive flux that tends to homogenize the milk concentrations is the product of the diffusivity and the local concentration gradient. Since the molecular diffusivity is constant, to a first-order approximation, two ways are left to increase the molecular fluxes

between milk and coffee, and thus to decrease the time until we can enjoy our coffee. First, we can increase the gradients, and second we can increase the contact surface between milk and coffee. This is exactly what happens when we stir the coffee: the straining of the initial milk drop creates a highly distorted geometry with a large contact surface and sharp gradients. In this situation, molecular effects become strong enough to smooth these features by molecular diffusion. This effect works so efficiently that a few seconds after stirring all milk and coffee gradients have vanished: the coffee is "well-mixed".

A little computation helps quantifying these effects. Imagine our cup contains initially 50% milk and 50% coffee in a way that both are horizontally homogeneous, and thus only depend on the vertical coordinate z and time t. The vertical diffusive spreading of the milk concentration m in our coffee cup would then be described by the classical one-dimensional diffusion equation of the form

$$\frac{\partial m}{\partial t} = \nu' \frac{\partial^2 m}{\partial z^2} \tag{1.1}$$

with ν' denoting the molecular diffusivity of milk in coffee (an analogous equation holds for the spreading of coffee in milk). Let's assume an initial distribution for the milk concentration of the form

$$m_0(z) = \frac{1}{2}\left(1 + \cos\left(\frac{n\pi z}{D}\right)\right), \tag{1.2}$$

where n is a positive integer, and D the thickness of the fluid inside the cup. For $n = 1$, the fluid is unstirred, and we only have a single layer of milk underneath the coffee layer (see red line in top panel of Figure 1.1). Increasing n may be viewed as a simple model for a stirring process that creates an increasing number of interfaces between milk and coffee. For $n = 10$ (middle panel), the stirring process has created 10 such interface, and for $n = 100$ (bottom panel) 100 interfaces can be defined. It should be clear that in a real coffee cup, the stirring process induces milk patches and streaks that are highly distorted and three-dimensional. Nevertheless, our simple one-dimensional model is sufficient to illustrate the basic effects of stirring and mixing as shown in the following.

To investigate the temporal evolution of the milk layers as a result of mixing, we insert an ansatz of the form

$$m(z,t) = \frac{1}{2}\left(1 + a(t)\cos\left(\frac{n\pi z}{D}\right)\right) \tag{1.3}$$

into (1.1), where $a(t)$ denotes the dimensionless amplitude of the milk concentration with $a(0) = 1$. This yields a differential equation of the form

$$\frac{\mathrm{d}a(t)}{\mathrm{d}t} = -\frac{a(t)}{\tau}, \tag{1.4}$$

where $\tau = D^2/(\nu' n^2 \pi^2)$ combines all parameters of the problem. The solution of (1.4) is of the form

$$a(t) = e^{-\frac{t}{\tau}}, \tag{1.5}$$

which reveals that τ plays the role of a *mixing time scale*.

The blue lines shown in Figure 1.1 (see the figure caption for the parameters chosen) illustrate the behavior of the solution found above for different values of n. For $n = 1$ (no stirring, top panel) the effect of mixing is seen to be negligble after a period of one minute. If some gentle stirring is applied (using the spoon) such that n is increased to 10, considerable mixing effects can be seen already after one minute (middle panel of Figure 1.1). Only intensive mixing ($n = 100$) leads to the desired result of (almost) complete mixing (bottom panel). For the parameters chosen, the mixing time scale is about $\tau = 10000$ s for the case of no stirring ($n = 1$), $\tau = 100$ s for little stirring ($n = 10$), and $\tau = 1$ s for strong stirring ($n = 100$).

Evidently, stirring is able to strongly increase the rate at which coffee and milk are mixed in our little experiment. One reason for this effect is the increase of the molecular fluxes due to increased vertical gradients. This is easiest understood from the Fickian law, a first principle in fluid mechanics that states that the molecular flux is proportional to the concentration gradient:

$$F = -\nu' \frac{\partial m}{\partial z} = \nu' \frac{n\pi}{2D} a(t) \sin \frac{n\pi z}{D} \ , \tag{1.6}$$

where in the second step we have used (1.3) and (1.5). For constant amplitude $a(t)$, the maximum diffusive flux (observed in the center of the interfaces) is seen to increase linearly for increasing n. A second effect leading to increased mixing is of purely geometric nature. This is easily seen from the fact that the increasing number of layers induced in our simple stirring problem also increases the overall contact surface between milk and coffee, which leads to larger mixing rates. Since both mechanisms depend linearly on n, their combined effect results in the quadratic dependency on n of the mixing time scale τ found above. The same mechanisms lead to increased mixing rates also in many other turbulent flows, in which scalar concentrations are stirred by turbulent motions.

We thus have identified two mechanisms that are essential for turbulent mixing: *Stirring* as a result of the complex straining patterns in a turbulent fluid increases the gradients and the contact surface until *mixing* starts reducing these gradients again by molecular effects. Mixing in the ocean works in a similar way, with the only difference that turbulent motions, rather than being created by tea spoons, are created by various types of flow instabilities. A typical example is the so-called Kelvin-Helmholtz instability displayed in Figure 1.1. In this flow, an initially purely horizontal interface separating dense and less dense fluid becomes unstable due to the vertical shear across the interface. Clearly seen is the distortion of the originally smooth interface after the instability has fully developed, leading to a strong increase of isopycnal surfaces (i.e. surfaces with constant densities) separating the fluids. This favors molecular diffusion, eventually leading to the generation of mixed fluid indicated by yellow-shaded regions in Figure 1.1.

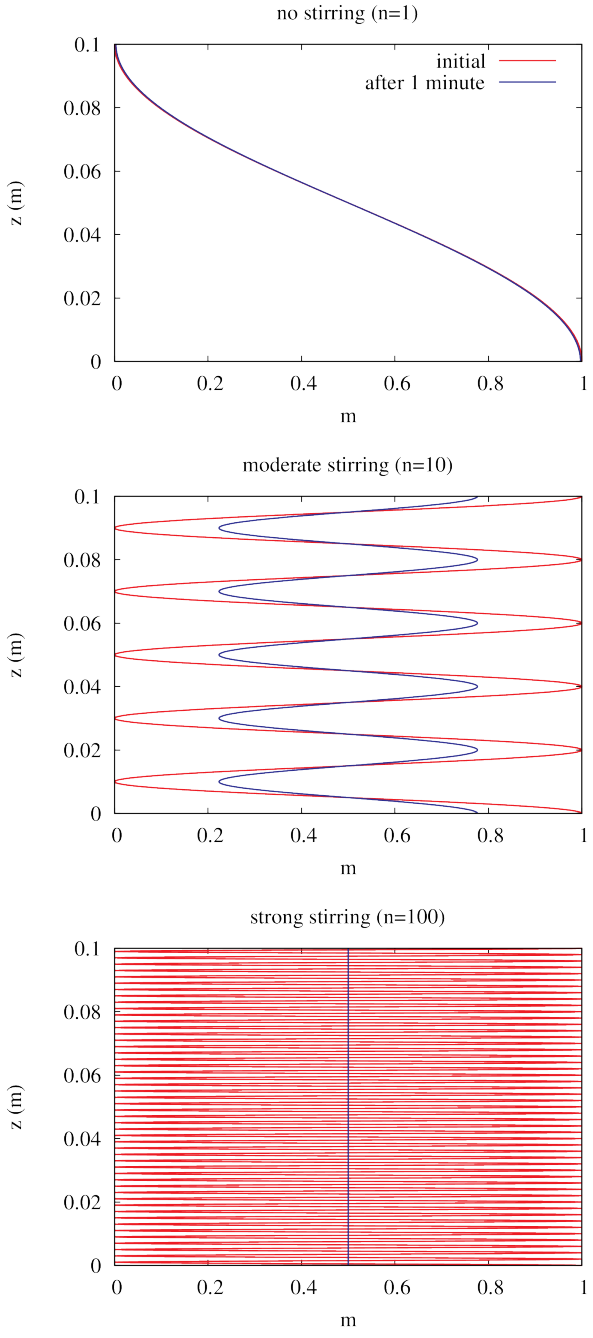

Figure 1.1: Evolution of the milk concentration m for the case of no stirring (top panel), little stirring (middle panel), and strong stirring (bottom panel). The initial distribution is shown as red line, and the distribution after 1 minute is shown a a blue line. The parameters for the problem are chosen as $D = 0.1$ m, and $\nu' = 10^{-7}\text{m}^2\ \text{s}^{-1}$.

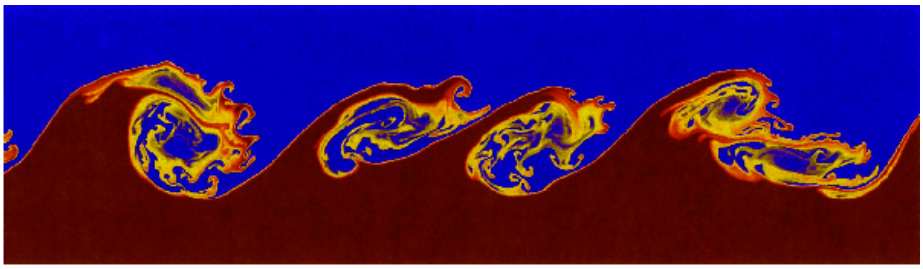

Figure 1.2: Evolution of turbulence along the interface of two fluids with different densities (red fluid is denser). Initial condition is a strongly sheared horizontal interface (the blue fluid moved to the right, while the red fluid moves to the left). This type of instability is called a Kelvin-Helmholtz instability.

1.2 How important is turbulence for mixing in the ocean?

The importance of turbulence for mixing in the ocean is best demonstrated by ignoring it for the moment. Similar to our cup of coffee (without stirring), we assume that the vertical spreading of heat in the ocean is purely a result of vertical molecular diffusion. This implies, analogously to the diffusion equation for milk in (1.1), that the evolution of temperature θ is described by a one-dimensional diffusion equatin of the form

$$\frac{\partial \theta}{\partial t} - \nu' \frac{\partial^2 \theta}{\partial z^2} = 0 \ , \tag{1.7}$$

where z and ν' denote the vertical coordinate and the molecular diffusivity of heat, respectively. The transport of salinity and other tracers is governed by analogous equations, however, with ν' replaced by the corresponding diffusivities such that the following results can be directly transferred.

For this idealized example, we consider an infinitely deep ocean $(-\infty < z \leq 0)$, and assume that the initial temperature distribution consists of an infinitely thin warm layer at the surface:

$$\theta = Q\delta(z) \quad \text{at } t = 0 \ , \tag{1.8}$$

where $\delta(z)$ denotes the Dirac delta distribution and Q is a constant. From the properties of the delta distribution, it follows that vertical integral of θ, which can be interpreted as the initial "heat content" of the water column, is equal to Q. At the upper boundary, we assume that the diffusive flux is zero, which is equivalent to the condition that the vertical temperature gradient vanishes:

$$\frac{\partial \theta}{\partial z} = 0 \quad \text{at } z = 0 \quad . \tag{1.9}$$

It is important to note that this boundary condition implies that the heat content Q in the water column remains constant over time, i.e. heat is only redistributed vertically by molecular diffusion.

An analytical solution for (1.7) can be constructed based on the Fourier integral,

$$\theta(z,t) = \frac{1}{2\pi}\int_{-\infty}^{\infty} e^{ikz} T(k,t)\,\mathrm{d}k \tag{1.10}$$

with $i = \sqrt{-1}$ and $T(k,t)$ denoting the Fourier amplitude at wave number k. Note that θ in (1.10) is generally a complex quantity. This will not bother us here because in the end, only the real part of our solution will be used.

Based in (1.10), the derivatives of θ may be expressed as

$$\frac{\partial\theta}{\partial t} = \frac{1}{2\pi}\int_{-\infty}^{\infty} e^{ikz}\frac{\partial T(k,t)}{\partial t}\,\mathrm{d}k\;, \tag{1.11}$$

and

$$\frac{\partial^2\theta}{\partial z^2} = \frac{1}{2\pi}\int_{-\infty}^{\infty} \left(-k^2\right) e^{ikz} T(k,t)\,\mathrm{d}k \quad . \tag{1.12}$$

This results in

$$\frac{\partial\theta}{\partial t} - \nu'\frac{\partial^2\theta}{\partial z^2} = \frac{1}{2\pi}\int_{-\infty}^{\infty} e^{ikz}\left(\frac{\partial T}{\partial t} + \nu' k^2 T\right)\,\mathrm{d}k = 0 \quad . \tag{1.13}$$

For arbitrary k, this equation can by satisfied only if

$$\frac{\partial T}{\partial t} + \nu' k^2 T = 0\;, \tag{1.14}$$

which has a well-known exponential solution of the form

$$T(k,t) = T(k,0)e^{-\nu' k^2 t} \quad . \tag{1.15}$$

The upper boundary condition is evaluated by inserting (1.15) into (1.10), taking the vertical derivative, and assuming that the result is zero at $z = 0$ as stated in (1.9). This yields an expression of the form

$$\frac{\partial\theta}{\partial z} = \frac{1}{2\pi}\int_{-\infty}^{\infty} T(k,0)ke^{-\nu' k^2 t}\,\mathrm{d}k = 0 \quad . \tag{1.16}$$

Because $ke^{-\nu' k^2 t}$ is an odd function of k, this condition can only be satisfied if $T(k,0)$ is a symmetric function of k. We will only consider the most simply case here, assuming $T(k,0) = T_0$, where T_0 is a constant determined below from the inital condition.

Using the fact that $e^{-\nu' k^2 t}$ is symmetric in k, and recalling the Euler relation for complex exponentials,

$$e^{iz} = \cos z + i\sin z\;, \tag{1.17}$$

(1.10) can be reformulated in the following more compact form:

$$\theta(z,t) = \frac{T_0}{\pi} \int_{-\infty}^{0} \cos(kz) e^{-\nu' k^2 t} \, \mathrm{d}k \quad . \tag{1.18}$$

Using standard integration tables, the integral on the right hand side of (1.18) can be shown to yield

$$\theta(z,t) = T_0 \sqrt{\frac{\nu'}{t}} \exp\left(-\frac{z^2}{4\nu t}\right) \quad . \tag{1.19}$$

We know from (1.8) and (1.9) that the vertical integral of θ is equal to Q for all times. From this condition, it can be shown that the vertical integral of (1.19) yields $T_0 = Q/\sqrt{\pi\nu'}$, such that (1.19) can be rewritten in the final form

$$\theta(z,t) = \frac{Q}{\pi\nu' t} \exp\left(-\frac{z^2}{4\nu' t}\right) \quad . \tag{1.20}$$

This is the classical solution of the diffusion equation with a pointwise initial heat distribution. In our context, (1.20) described the downward diffusion (or mixing) of heat initially contained inside an infinitely thin layer at the surface.

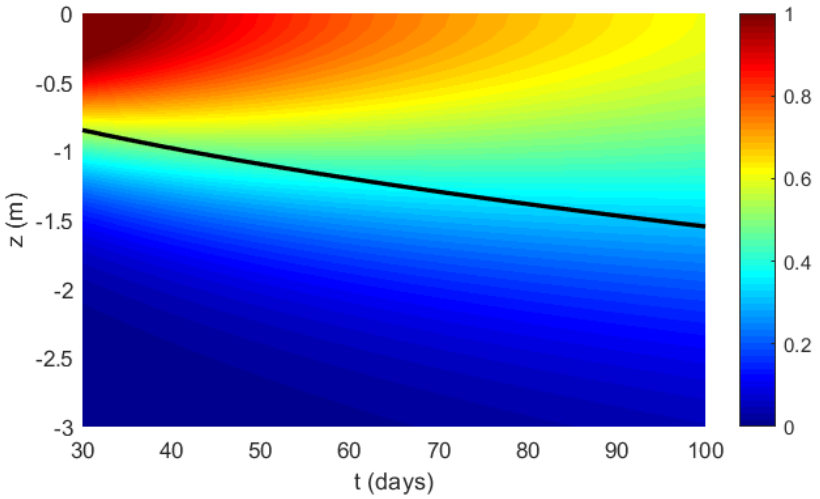

Figure 1.3: Solution (1.20) for $Q = 1$ and $\nu' = 10^{-7}$ m^2 s^{-1}. Temperature units are arbitrary. The black lines shows D_2 computed from (1.22).

As a measure for the penetration depth of diffusion, it is useful to compute the depth D_2 at which θ has decayed to half its surface value:

$$\frac{1}{2} = \frac{\theta(-D_2,t)}{\theta(0,t)} = \exp\left(-\frac{D_2^2}{4\nu' t}\right) \ , \tag{1.21}$$

which is equivalent to

$$D_2 = 2\sqrt{-\nu' t \ln 0.5} \quad . \tag{1.22}$$

The solution (1.20) for $Q = 1$ and $\nu' = 10^{-7}$ m^2 s^{-1} (this is a typical value for the diffusivity of heat) is shown in Figure 1.3. The main conclusion from this is that, even over a period as long as 100 days, heat diffusives downward not more than a few meters. Figure 1.3 also shows that the time required to double the penetration depth is of the order of 70 days in this example.

These results are in drastic contrast to the real time scales required for the downward mixing of heat in the near-surface region of the ocean. This is illustrated with an example in Figure 1.4, showing that the warm surface layer doubles its thickness within hours during the passage of a strong wind event.

We conclude that purely molecular diffusion cannot, not even rudimentarily, describe the observed vertical redistribution of heat in the ocean. This statement also applies for the vertical transport of momentum and dissolved substances (e.g., salt) because their molecular diffusion is also governed by equations of the same form as (1.7), however, with modified molecular diffusion coefficients.

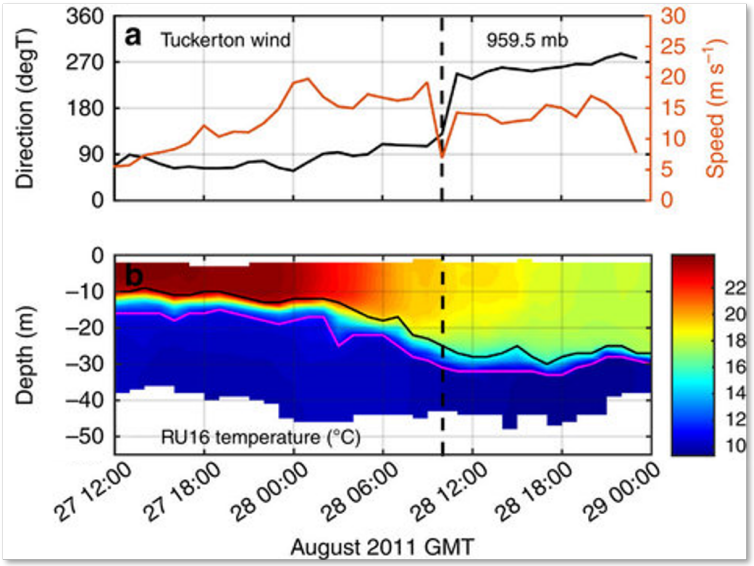

Figure 1.4: Shown are (a) wind speed and direction, and (b) near-surface temperature at a station in the Mid-Atlantic Bight during the passage of hurricane "Irene". Figure taken from Glenn et al. (2016).

1.3 Observational evidence of turbulence

1.3.1 Laboratory experiments

In 1883, Osborne Reynolds described an experiment on the transition between laminar and turbulent flow in a tube. He discovered that the flow resistance was proportional to the flow velocity for small velocities, and proportional to the square of the flow velocity, V, if a certain threshold was exceeded. He found that this critical velocity depended on the diameter, D, of the tube and the viscosity, ν, of the water. He further noticed by visual inspection of streaks of colored water that, at this critical velocity, a transition from *direct* (straight, laminar) to *sinuous* (turbulent) motion took place, see figure 1.5.

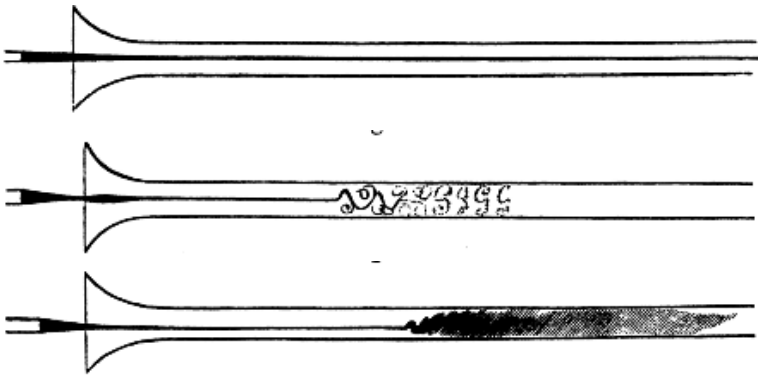

Figure 1.5: Osborn Reynold's experiment. Laminar (top panel), transitional flow (middle panel), and fully turbulent flow (bottom panel). The current flows from left to right through a glass tube, with some fluid marked by streaks of colored water.

Reynolds found in his tube experiments that the non-dimensional number

$$Re = \frac{DV}{\nu} \,, \tag{1.23}$$

which was later, to his honour, named the *Reynolds number*. For Re smaller than 1900, he found laminar flow, whereas for Re larger than 2000, the flow showed a transition to irregular turbulent motions.

Another interesting laboratory experiment demonstrating the evolution of instabilities and finally turbulence consists of a uniform, plane flow around a circular cylinder. For very low flow velocities, the flow is laminar and symmetrically arranged around the cylinder with streamlines smoothly aligned. With increasing velocities, a von Kármán vortex street of alternating vortices develops in the wake of the cylinder (Figure 1.6). And for even higher flow velocities, the flow behind the cylinder becomes fully turbulent.

Also for this experiment, the parameter defined in (1.23) describes the transition to turbulence, provided D is identified now with the diameter of the cylinder, and V with the uniform flow speed upstream of the cylinder. The wake behind the cylinder develops for $Re > 10$, the Kármán vortex street for $Re > 100$. For Re larger than 1000, the flow becomes turbulent.

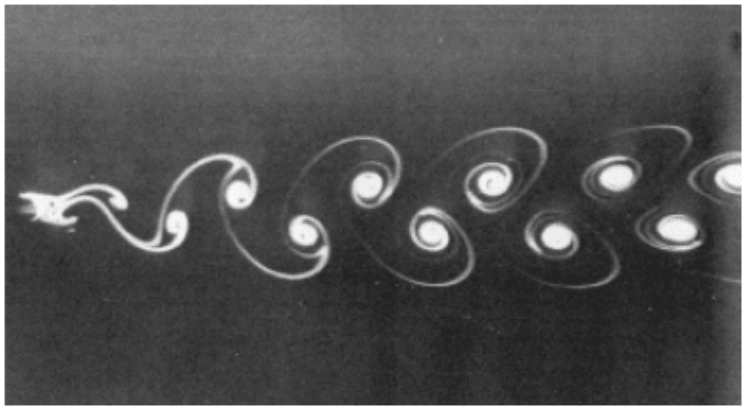

Figure 1.6: Evolution of a Kármán vortex street in the wake of a cylinder. The flow is uniform from the left. The cylinder is near the left edge of the figure, not directly visible in this plot. Ink has been injected a small distance upstream of the cylinder to visualize the fluid motion.

Generalizing the above results, we note that for all incompressible, unstratified flows with one single relevant length scale $\mathcal{L}$, and one single relevant flow speed $\mathcal{V}$, a generalized Reynolds number of the form

$$Re = \frac{\mathcal{V}\mathcal{L}}{\nu} \tag{1.24}$$

can be defined. Since under these assumptions, no other dimensional quantities enter the problem, Re is the only non-dimensional parameter than can be constructed from these. It follows that the Reynolds number alone describes the transition from laminar to turbulent flows. In spite of many different geometries that have been investigated in this way, it turns out that transition typically occurs for $Re = \mathcal{O}(10^3)$.

Similar to the laboratory studies discussed above, estimates of the Reynolds number can also be derived for oceanic flows. It should be recalled, however, that Re described the transition to turbulence only for the conditions summerarized in the context of (1.24). As an example, let's consider a non-rotating, incompressible, unstratified, horizontally homogeneous oceanic flow of depth H and a characteristic (e.g. vertically averaged) velocity V. For typical values found in shallow coastal flows ($H = 20$ m, $V = 0.2\ \mathrm{m\,s^{-1}}$, $\nu = 10^{-6}\mathrm{m^2 s^{-1}}$), we

compute $Re = 4 \times 10^6$. This is clearly above the threshold for transition to turbulence, supporting our previous speculation (see Section 1.2) that unstratified oceanic flows are turbulent. In the following, we will investigate a few direct manifestations of turbulence in small-scale data sets of oceanic flows.

1.3.2 Oceanic observations

Let us first investigate the small-scale velocity structure of oceanic mixing layers[1]. Small-scale velocity fluctuations can be measured by so-called microstructure profilers using an airfoil-shaped shear probe (a few millimeters long), sensing transverse velocity fluctuations caused by turbulent eddies, while the profiler is passing through the fluid.

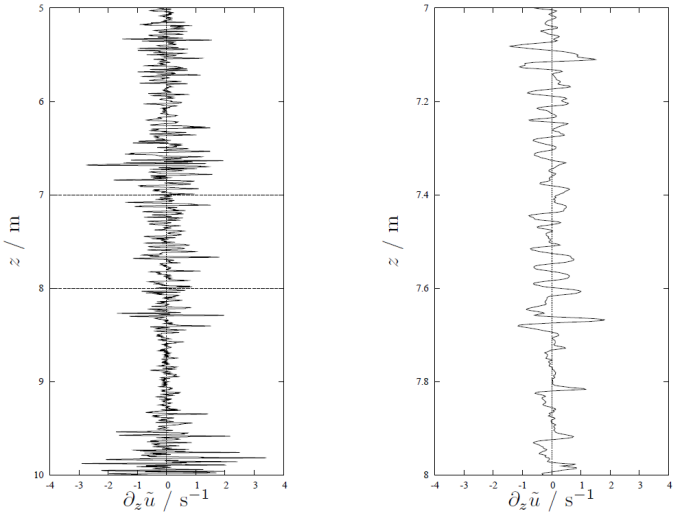

Figure 1.7: Vertical shear of the horizontal velocity measured by a freely falling shear microstructure profiler in the mixed layer of the Northern Baltic Sea. Left panel: profile over a range of 5 m; right panel: enlarged version of the same profile. Courtesy of Adolf Stips, Ispra (Italy).

An example for such an observation is given in Figure 1.7, showing the small-scale vertical velocity shear in the upper mixed layer of the Baltic Sea. On the scale of the mixed layer depth, the profile looks very spiky, indicating intense small-scale turbulence. However, on the scale of a few centimeters (right panel), we see that the profile is in fact smooth. This is the scale at which the

[1] Just for later reference: a *mixed layer* is defined in the sense that the vertical gradients of various properties like temperature and salinity are very small. It may have been generated by a previous mixing event, or may be actively turbulent at the moment. In contrast to that, a *mixing layer* is always turbulent (thus mixing) but it may or may not exhibit vertical density gradients.

irreversible conversion of turbulent kinetic energy into internal energy (heat) by viscous effects takes place. Similar to the scalar mixing experiment in the coffee cup discussed above, turbulence has created small-scale gradients that are strong enough to be directly affected by molecular smoothing: viscous effects set the lower threshold for the scales of turbulent motions. The difference is that, here, velocity fluctuations are mixed, rather than milk and coffee fluctuations.

A similar mechanisms also applies to scalar flucations. Figure 1.8 shows a high-resolution temperature profile obtained from a temperature microstructure sensor (a fast-response thermistor) mounted on an autonomous profiling platform in the central Baltic Sea. The depth range shown here corresponds to an intermediate water depth that is not directly affected by the wind forcing. Different from the surface layer shown in the previous example, these deeper regions in the Baltic Sea are therefore typcially non-turbulent. However, occasionally local turbulent bursts due to Kelvin-Helmholtz instabilities are observed (we have alread encountered this important type of flow instability in the context of Figure 1.1). The example in Figure 1.8 reveals centimeter-scale temperature fluctuations in the central region of the instability that are indicative for turbulence. Similar to the previous example, the scales of these flucuations are small enough to be directly affected by molecular diffusion, which tends to smooth them and thus reduce the overall temperature variance.

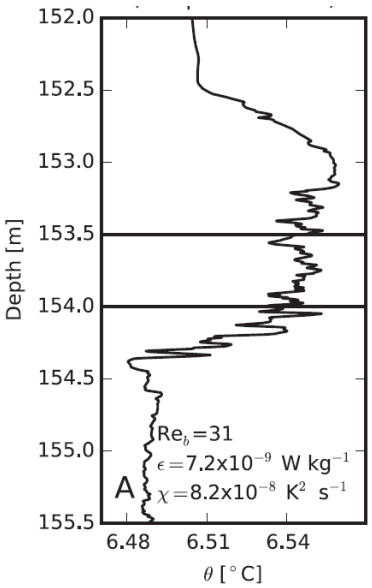

Figure 1.8: High-resolution temperature structure inside a Kelvin-Helmholtz instability observed in the central Baltic Sea with temperature microstructure sensors mounted on an autonomous profiling platform (the instrument is described at https://www.io-warnemuende.de/GODESS.html).

Our final example is from shallow coastal waters at the east coast of North America. This data set has been obtained with the help of Particle Image Velocimetry (PIV), a technique that is normally only used in laboratory settings. Here, natural particles (e.g., zooplankton and suspenced sediment) are illuminated by a laser sheet. From double-exposure photographs, taken with a small time difference, particle velocities can be computed from the spatial shift of individual particles that can be traced. Assuming that particles move passively with the water, vector maps, like the one shown in Figure 1.9, can be constructed. Beyond the capabilities of microstructure profilers, this technique allows to observe the two-dimensional structure of turbulence. In this example, we see that a small vortex of only 5 cm diameter seen in the center of the left panel has been advected by the mean flow (or larger turbulent motions) to the right edge of the right panel, and another vortex has entered from the left edge of the left panel. PIV is, however, an expensive technique, and has only rarely been applied in real oceanic flows. Apart from this, its main disadvantage is related to the fact that light is absorbed quickly in the water, limiting the sampling range of this technique to a few meters only.

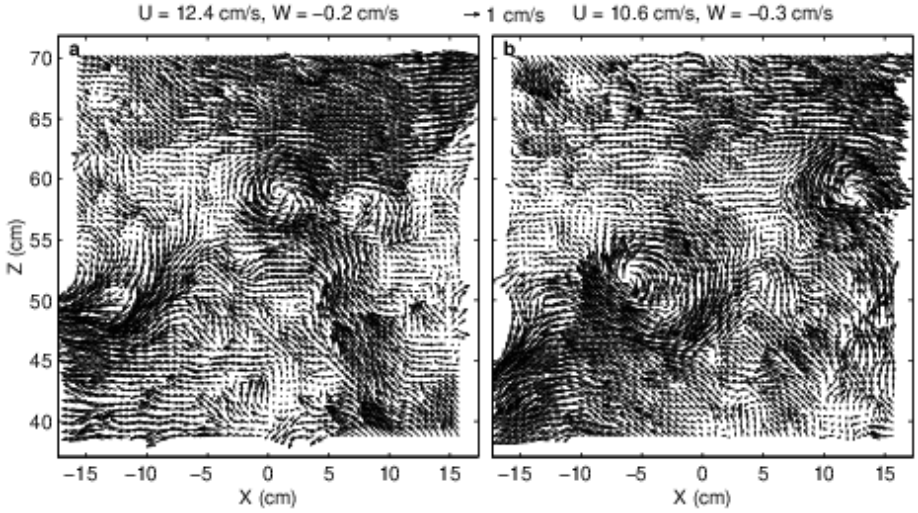

Figure 1.9: Two velocity vector maps of the same area, sampled 1 s apart. The instantaneous mean velocity of the sample area (shown at the top of each map) is subtracted from each vector to highlight the turbulence structure. The vertical coordinates represent the actual distance from the bottom. These frames were observed by means of Particle Image Velocimetry (PIV) near the LEO-15 site off the coast of New Jersey in 15 to 21 m depth of water. Figure by Alex Nimmo Smith (Plymouth, England).

1.4 Definition of turbulence

It has often been pointed out that it is difficult to provide a precise definition of turbulence. Based on the previous examples, it is, however, possible to summarize a few properties that are common to all turbulent flows that we are interested in here.

1. *Randomness:* Turbulent flows generate stochastic data sets both in time and in space. Small uncertainties in the initial and boundary conditions quickly amplify, rendering a deterministic description of individual turbulent fluctuations impossible. Often possible is, however, the prediction of statistical quantities (statistical moments, correlations, probability distributions).

2. *Increased transport and mixing:* Turbulent flows generally show strongly increased mixing and transport rates of matter, heat, and momentum. As shown above, the reason for this is the generation of sharp gradients and increased contact surfaces due to the complex strain field associated with the turbulent motions.

3. *Vorticity:* Turbulent flows are characterized by vorticity, manifested in the omnipresence of eddying motions. These vortices (often called "eddies" in oceanography) involve a wide range of spatial wave lengths, ranging from the largest scales imposed by the bounding geometry down to the smallest scales, where eddies are dissipated due to molecular (viscous) smoothing.

4. *Dissipation:* Turbulence is "dissipative", meaning that kinetic energy is dissipated into heat due to viscous friction at the smallest scales. Similarly, also scalar fluctuations are smoothed (or dissipated) be molecular diffusion, implying that the overall scalar variance is reduced (see our coffee example). Thus, a mechanism must exist transporting energy and scalar variance from the largest scales, where they are introduced to the system, towards the smallest scales, where they are dissipated. As shown in later sections, this mechanism is tightly connected to the non-linear advection terms in the transport equations.

Chapter 2

Equations of Motion

Different from most other areas of physics, the equations describing so-called Newtonian Fluids, including dry air and water, are known. With increasing computational power and improved numerical methods this has opened a way to directly simulate turbulent flows with the help of high-performance computing systems. Such *Direct Numerical Simulations (DNS)* are generally considered to be equivalent to laboratory experiments, and have in fact replaced them in many cases. In the following, we will therefore briefly review these equations, usually referred to as the Navier-Stokes Equations, which form the starting point of all following chapters. A more in-depth discussion of the background and derivation of Navier-Stokes Equations may be found in numerous available textbooks on fluid mechanics, e.g. in Kundu and Cohen (2008).

2.1 Navier-Stokes equations

The key underlying physical principle for the derivation of the Navier-Stokes Equations is the momentum budget, which is the fluid mechanical version of Newton's second law. In symbolic notation this equation can be written as

$$\frac{\partial \boldsymbol{u}}{\partial t} + \boldsymbol{u} \cdot \nabla \boldsymbol{u} + 2\boldsymbol{\Omega} \times \boldsymbol{u} = \frac{1}{\rho_0} \nabla \cdot \boldsymbol{T} + \frac{\rho}{\rho_0} \boldsymbol{g} \,, \tag{2.1}$$

where $\boldsymbol{u}$ is velocity, $\boldsymbol{g}$ the gravity vector, ρ density, and ρ_0 a constant reference density. $\boldsymbol{T}$ denotes the stress tensor, and the term $2\boldsymbol{\Omega} \times \boldsymbol{u}$ represents the Coriolis acceleration with $\boldsymbol{\Omega}$ denoting Earth's rotation. In (2.1), we have assumed that the density is constant everywhere, except in the buoyancy term on the right hand side. This is called the *Boussinesq* approximation, which is widely used in geophysical fluid mechanics. As a consequence of the Boussinesq assumption, the *balance of mass* adopts the particularly simple form of an incompressible fluid:

$$\nabla \cdot \boldsymbol{u} = \boldsymbol{0} \,, \tag{2.2}$$

which is referred to as the *continuity equation* in the following.

For a Newtonian fluid, the *stress tensor* appearing in (2.1) follows from the *Cauchy-Poisson Law*. Under the additional assumption that the fluid is incompressible (or Boussinesq) this relation can be expressed as

$$\frac{1}{\rho_0}\boldsymbol{T} = -\frac{p}{\rho_0}\boldsymbol{I} + 2\nu\boldsymbol{S}\ , \tag{2.3}$$

where $\boldsymbol{I}$ is the unit tensor (δ_{ij} in indical notation), p the pressure, ν the kinematic viscosity (or diffusivity of momentum), and $\boldsymbol{S}$ the rate of strain tensor. The latter is defined in component form as the symmetric part of the velocity gradient

$$S_{ij} = \frac{1}{2}\left(\frac{\partial u_i}{\partial x_j} + \frac{\partial u_j}{\partial x_i}\right) \quad . \tag{2.4}$$

Inserting (2.3) into the momentum budget in (2.1) results in

$$\frac{\partial \boldsymbol{u}}{\partial t} + \boldsymbol{u}\cdot\nabla\boldsymbol{u} - \nu\nabla^2\boldsymbol{u} + 2\boldsymbol{\Omega}\times\boldsymbol{u} = -\frac{1}{\rho_0}\nabla p + \frac{\rho}{\rho_0}\boldsymbol{g}\ , \tag{2.5}$$

where we have used the continuity equation (2.2) to simplify the frictional term. This coupled set of three equations is usually referred to as the *Navier-Stokes equations*. The overwhelming success in describing turbulent flows with these equations is related to the fact that the material law in (2.3) has been shown to describe the behavior of viscous gases and simple fluids like water with almost perfect accuracy.

In component form, the Navier-Stokes equations can be written as

$$\frac{\partial u_i}{\partial t} + u_j\frac{\partial u_i}{\partial x_j} - \nu\frac{\partial^2 u_i}{\partial x_j \partial x_j} + 2\varepsilon_{ijk}\Omega_j u_k = -\frac{1}{\rho_0}\frac{\partial p}{\partial x_i} + \frac{g_i}{\rho_0}\rho \quad . \tag{2.6}$$

Here, $u_1 = u$, $u_2 = v$ and $u_3 = w$ are the eastward, the northward and the upward velocity components, respectively. The gravity vector is defined as $\boldsymbol{g} = (0, 0, -g)$, and Earth's rotation is split into components towards North and geoid-normal: $\boldsymbol{\Omega} = (0, \Omega\cos(\Phi), \Omega\sin(\Phi))$ where $\Omega \approx 7.3{\cdot}10^{-5}$ s^{-1} is the angular velocity of the Earth, and Φ is latitude. For water, the kinematic viscosity ν has a value of $\nu = 1.3\cdot 10^{-6}$ m^{2}s^{-1} at 10°C, which varies with temperature such that its value decreases to $\nu = 8.0\cdot 10^{-7}$ m^{2}s^{-1} at 30°C.

2.1.1 Scaling

In order to investigate the relative importance of individual terms in the Navier-Stokes equation, let us assume that the turbulent flow patterns we are interested in have a typical velocity scale $\mathcal{U}$, and a typical length scale $\mathcal{L}$. To find an appropriate scale also for the pressure, it is useful to first subtract the (dominating) hydrostatic contribution $\bar{p}(z) = -zg\rho_0$ to emphasize the dynamical effects on the pressure. Then, (2.6) can be re-written in terms of the residual pressure $\tilde{p} = p - \bar{p}$:

$$\frac{\partial u_i}{\partial t} + u_j\frac{\partial u_i}{\partial x_j} - \nu\frac{\partial^2 u_i}{\partial x_j^2} + 2\varepsilon_{ijl}\Omega_j u_l = -\frac{1}{\rho_0}\frac{\partial \tilde{p}}{\partial x_i} + \frac{g_i}{\rho_0}(\rho - \rho_0). \tag{2.7}$$

The pressure component $\tilde{p}$ includes the effect of velocity fluctuations, scaling according to the well-known Bernoulli relation with $\rho_0 \mathcal{U}^2$. If we further denote the scale of typical density fluctuations as $\Delta\rho$, and assume the changes in time are dominated by advection, we can define the following set of *non-dimensional* parameters:

$$\begin{aligned} \hat{u}_i &= \frac{u_i}{\mathcal{U}}, \qquad \hat{x}_i = \frac{x_i}{\mathcal{L}}, \qquad \hat{t} = t \cdot \frac{\mathcal{U}}{\mathcal{L}}, \\ \hat{p} &= \frac{\tilde{p}}{\rho_0 \mathcal{U}^2}, \quad \hat{\rho} = \frac{\rho - \rho_0}{\Delta\rho}, \quad \hat{\Omega}_i = \frac{\Omega_i}{\Omega}, \end{aligned} \tag{2.8}$$

The key observation here is that, provided we have picked the scales correctly, all non-dimensional quantities are of order one. After inserting (2.8) into (2.7), we obtain the Navier-Stokes equations in the form

$$\frac{\partial \hat{u}_i}{\partial \hat{t}} \cdot \frac{\mathcal{U}^2}{\mathcal{L}} + \hat{u}_j \frac{\partial \hat{u}_i}{\partial \hat{x}_j} \cdot \frac{\mathcal{U}^2}{\mathcal{L}} - \nu \frac{\partial^2 \hat{u}_i}{\partial \hat{x}_j^2} \cdot \frac{\nu \mathcal{U}}{\mathcal{L}^2} + 2\varepsilon_{ijl} \hat{\Omega}_j \hat{u}_l \cdot \Omega \mathcal{U} = -\frac{\partial \hat{p}}{\partial \hat{x}_i} \cdot \frac{\mathcal{U}^2}{\mathcal{L}} + \hat{\rho} g_i \frac{\Delta\rho}{\rho_0} \quad . \tag{2.9}$$

Dividing by $\mathcal{U}^2/\mathcal{L}$, the equations can be derived in non-dimensional form

$$\frac{\partial \hat{u}_i}{\partial \hat{t}} + \hat{u}_j \frac{\partial \hat{u}_i}{\partial \hat{x}_j} - \frac{\partial^2 \hat{u}_i}{\partial \hat{x}_j^2} \cdot \frac{\nu}{\mathcal{U}\mathcal{L}} + 2\varepsilon_{ijl} \hat{\Omega}_j \hat{u}_l \cdot \frac{\Omega \mathcal{L}}{\mathcal{U}} = -\frac{\partial \hat{p}}{\partial \hat{x}_i} - \hat{\rho} \cdot \frac{g \Delta\rho}{\rho_0} \frac{\mathcal{L}}{\mathcal{U}^2} \delta_{i3} \ , \tag{2.10}$$

where two observations should be made clear: First, the non-dimensional equations (2.10) contain exactly the same information as the original set in (2.6) because we have not use any additional assumptions in deriving them. Second, all terms with a hat are of order one such that individual terms can now be conveniently compared by investigating the factors multiplying them.

To this end, it is customary to re-write these factors in terms of the Reynolds number (1.24), and the so-called Rayleigh number defined as

$$R_a = g \frac{\Delta\rho}{\rho_0} \frac{\mathcal{L}^3}{\nu^2} \quad . \tag{2.11}$$

The Rayleigh number represents the (square of) the ratio between the buoyancy and viscous forces acting on the fluid. Using these definitions, we finally obtain from (2.10) a non-dimensional relation of the form

$$\frac{\partial \hat{u}_i}{\partial \hat{t}} + \hat{u}_j \frac{\partial \hat{u}_i}{\partial \hat{x}_j} - \frac{\partial^2 \hat{u}_i}{\partial \hat{x}_j^2} \cdot \frac{1}{R_e} + 2\varepsilon_{ijl} \hat{\Omega}_j \hat{u}_l \cdot \frac{\Omega \mathcal{L}}{\mathcal{U}} = -\frac{\partial \hat{p}}{\partial \hat{x}_i} - \frac{R_a}{R_e^2} \hat{\rho} \delta_{i3} \quad . \tag{2.12}$$

The first two terms on the left hand side, and the first term on the right hand side do not depend any more on the scaling factors: they are of order one as pointed out above. The frictional term (third term on right hand side) becomes small for a large Reynolds number, which is a manifestation of the fact that R_e physically represents the ratio of inertial and viscous forces. We will see below that in turbulent flows R_e is usually very large except for the smallest turbulent motions.

The fourth term on the right hand side (Coriolis acceleration) is scaled with $\Omega\mathcal{L}/\mathcal{U}$. For shallow mixed layers with $\mathcal{L} \approx 10$ m and typical large-scale turbulent velocities $\mathcal{U} \approx 0.1\ \mathrm{m\,s^{-1}}$, we obtain $\Omega\mathcal{L}/\mathcal{U} \approx 0.007$, which means that Earth's rotation is negligible at these scales. It turns out that, apart from very few exceptions like deep convection, the effect of system rotation can be ignored when studying three-dimensional turbulence in oceanic applications.

Since we generally have $R_e \gg 1$ in flows of geophysical interest, the last term of (2.10) will play a significant role only if the Rayleigh number is very large. Due to the factor ν^{-2} in (2.11) this is, however, very often the case.

Finally, it should be pointed out that the scaling relations used here only apply for three-dimensional turbulent motions at the scales mentioned above. We have seen in the Hydrodynamics lecture that geophysical large-scale motions obey different scaling relations in which the effect of rotation is much more pronounced.

2.1.2 Elimination of pressure

For an incompressible (or Boussinesq) fluid obeying the continuity equation (2.2), the pressure becomes a free variable that can be derived from the velocity and density fields. This is easiest understood by considering the divergence of the Navier-Stokes equation (2.6):

$$\frac{\partial}{\partial t}\frac{\partial u_i}{\partial x_i} + \frac{\partial}{\partial x_i}u_j\frac{\partial u_i}{\partial x_j} - \nu\frac{\partial}{\partial x_i}\frac{\partial^2 u_i}{\partial x_j \partial x_j} + 2\varepsilon_{ijk}\Omega_j\frac{\partial u_k}{\partial x_i} = -\frac{1}{\rho_0}\frac{\partial^2 p}{\partial x_i \partial x_i} + \frac{g_i}{\rho_0}\frac{\partial \rho}{\partial x_i} \quad . \tag{2.13}$$

Using (2.2), it is straightforward to show that the first and third terms on the left hand side vanish, and that (2.13) can thus be rearranged to yield

$$\frac{\partial^2 p}{\partial x_i \partial x_i} = -\rho_0\frac{\partial u_j}{\partial x_i}\frac{\partial u_i}{\partial x_j} - 2\varepsilon_{ijk}\rho_0\Omega_j\frac{\partial u_k}{\partial x_i} - g\frac{\partial \rho}{\partial x_3} \quad . \tag{2.14}$$

This equation is recognized as an Poisson equation for the pressure. The solution of this type of partial differential equations is known to depend on the entire domain, which mirrors the fact that in incompressible or Boussinesq fluids sound waves travel at infinite speed, communicating pressure signals instantly.

Note that (2.14) replaces the continuity equation (2.2), which was involved in its derivation. Thus, one way of interpreting (2.14) is that this equation determines the pressure always exactly such that the velocity field is divergence free. Numerical schemes generally exploit this fact to correct the velocity field obtained from time-stepping (2.6) by a pressure correction that guarantees zero divergence.

2.1.3 Kinetic energy from the Navier-Stokes equation

A dynamic equation for the kinetic energy per unit mass,

$$E = \frac{1}{2}u_i u_i \ , \tag{2.15}$$

is obtained by scalar multiplication of (2.1) with the velocity vector $\boldsymbol{u}$, and subsequent insertion of the Cauchy-Poisson material law (2.3). As shown in the assignments, the result can be written as

$$\frac{\partial E}{\partial t} + u_i \frac{\partial E}{\partial x_i} - 2\frac{\partial \nu u_i S_{ij}}{\partial x_j} + \frac{1}{\rho_0}\frac{\partial u_i p}{\partial x_i} = -2\nu S_{ij} S_{ij} + \frac{\rho}{\rho_0} u_i g_i \quad . \tag{2.16}$$

Note that the Coriolis term does not appear any more in this equation.

The meaning of the different terms in (2.16) is as follows. On the left hand side, the rate term is balanced by advection (second term), viscous transport (third term), and pressure transport (fourth term). On the right hand side, the first term is seen to be strictly negative, and represents dissipation rate, i.e. the irreversible conversion of kinetic energy into internal energy by molecular friction. The last term quantifies the work done against gravity. It may also be interpreted as a conversion from kinetic energy to potential energy, or vice-versa.

2.1.4 Vorticity equation

As shown in the Hydrodynamics lecture, the *vorticity*

$$\boldsymbol{\omega} = \nabla \times \boldsymbol{u} = \varepsilon_{ijk} \frac{\partial u_k}{\partial x_j} \boldsymbol{e}_i \tag{2.17}$$

is directly related to the angular velocity of a fluid element. More specifically, the component ω_1 can be shown to correspond to (twice) the rate of rotation of a fluid element around $\boldsymbol{e}_1$; analogous relations hold for the other coordinate directions.

A transport equation for $\boldsymbol{\omega}$ can be obtained by taking the curl of the Navier-Stokes equations in (2.6). Since the derivations are somewhat lengthy we will use in the following the short-hand notation $\partial/\partial t \equiv \partial_t$ and $\partial/\partial x_i \equiv \partial_i$. As discussed above, system rotation is unlikely to affect oceanic turbulence in most situations, and therefore only the non-rotating case is considered here. Taking the curl of (2.6) yields in a first step

$$\partial_t \left(\varepsilon_{lmi}\partial_m u_i\right) + \varepsilon_{lmi}\partial_m \left(u_j \partial_j u_i\right) - \nu \varepsilon_{lmi}\partial_m \partial_{jj} u_i = -\frac{1}{\rho_0}\varepsilon_{lmi}\partial_m \partial_i p + \frac{g_i}{\rho_0}\varepsilon_{lmi}\partial_m \rho \quad . \tag{2.18}$$

Now let us consider individual terms in (2.18), starting with the rate terms that becomes

$$\partial_t \left(\varepsilon_{lmi}\partial_m u_i\right) = \partial_t \omega_l \tag{2.19}$$

and therefore represents the rate of change of vorticity. According to (A.47), the advection term in (2.6) can be re-expressed as

$$u_j \partial_j u_i = -\varepsilon_{ikj} u_k \omega_j + \frac{1}{2}\partial_i (u_j u_j) \ , \tag{2.20}$$

and the corresponding term in (2.18) thus becomes

$$-\varepsilon_{lmi}\partial_m \varepsilon_{ikj} u_k \omega_j + \frac{1}{2}\varepsilon_{lmi}\partial_m \partial_i (u_j u_j) \quad . \tag{2.21}$$

The second part is zero because it includes the contraction of a symmetric and a antisymmetric tensor (see assignment 1). The first part results in

$$\begin{aligned} -\varepsilon_{lmi}\varepsilon_{ikj}\partial_m u_k\omega_j &= \left(\delta_{lj}\delta_{mk}-\delta_{lk}\delta_{mj}\right)\partial_m(u_k\omega_j) \\ &= \partial_k\left(u_k\omega_l\right)-\partial_j\left(u_l\omega_j\right) \\ &= u_k\partial_k\omega_l+\omega_l\partial_k u_k-u_l\partial_j\omega_j-\omega_j\partial_j u_l \\ &= u_k\partial_k\omega_l-\omega_j\partial_j u_l, \end{aligned} \tag{2.22}$$

where the second and third term in the third line vanish due to (2.2) and (A.46), respectively. The viscous term expresses Laplacian diffusion of vorticity,

$$\nu\varepsilon_{lmi}\partial_m\partial_{jj}u_i=\nu\partial_{jj}\omega_l, \tag{2.23}$$

where we have used (A.48), and the pressure terms vanishes due to (A.44):

$$-\frac{1}{\rho_0}\varepsilon_{lmi}\partial_m\partial_i p=0 \quad . \tag{2.24}$$

Thus, in summary, after renaming dummy indices, we obtain the vorticity equation in the following form

$$\frac{\partial\omega_i}{\partial t}+u_j\frac{\partial\omega_i}{\partial x_j}=\omega_j\frac{\partial u_i}{\partial x_j}+\frac{1}{\rho_0}\varepsilon_{ijk}\frac{\partial\rho}{\partial x_j}g_k+\nu\frac{\partial^2\omega_i}{\partial x_j\partial x_j}\ , \tag{2.25}$$

or in vector notation:

$$\frac{\partial\boldsymbol{\omega}}{\partial t}+\boldsymbol{u}\cdot\nabla\boldsymbol{\omega}=\boldsymbol{\omega}\cdot\nabla\boldsymbol{u}+\frac{1}{\rho_0}\nabla\rho\times\boldsymbol{g}+\nu\nabla^2\boldsymbol{\omega} \quad . \tag{2.26}$$

Apart from the usual rate and advective transport terms on the left hand side, and the viscous transport term on the right hand side, we see that changes in vorticity are related to two generation or destruction mechanisms. The first term on the right hand side represents the effect vortex stretching and tilting, and the second the effect of stratification or "baroclinicity". Both effects are examined in more detail in the following.

Let us first consider the second term on the right hand side, $\nabla\rho\times\boldsymbol{g}$. If the horizontal gradients of density are zero, i.e. the density structure is horizontally homogeneous, then this cross product is zero because the two vectors are parallel. Only if the density gradient vector is not aligned with the vertical, i.e. if isopycnals (lines of constant density) are tilted, vorticity may be produced by gravitational acceleration. In that case, gravitation tries to turn isopycnals into the horizontal plane, a process which is producing vorticity.

If density is constant, the only vorticity generation mechanism is given by the term $\boldsymbol{\omega}\cdot\nabla\boldsymbol{u}$. First insight about its meaning can be gained by considering a purely two-dimensional flow with all motions taking place in a plane. In this case, the vorticity vector $\boldsymbol{\omega}$ points perpendicular to the two-dimensional plane,

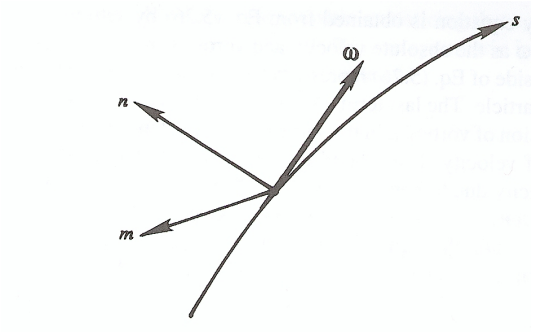

Figure 2.1: Coordinate system aligned with the vorticity vector. This figure has been taken from Kundu and Cohen (2008).

and is thus orthogonal to the velocity gradient which will lie inside the plane. The scalar product is zero in this case: $\boldsymbol{\omega} \cdot \nabla \boldsymbol{u} = \boldsymbol{0}$. We conclude that the mechanism associated with this term must three-dimensional.

To investigate this aspect more closely, let us consider the geometry depicted in Figure 2.1. Here, s denotes a curvilinear coordinate aligned with the direction of $\boldsymbol{\omega}$. Such coordinate lines are also referred to as *vortex lines*, completely analogous with the concept of *streamlines* that are locally aligned with $\boldsymbol{u}$. Further, we assume that m and n are the two other coordinates orthogonal to s, and orthogonal to each other. Further let $\boldsymbol{e}_s$, $\boldsymbol{e}_m$ and $\boldsymbol{e}_n$ be the corresponding unit base vectors. Then, $\boldsymbol{\omega} \cdot \nabla \boldsymbol{u}$ may be re-written as

$$\begin{aligned} \boldsymbol{\omega} \cdot \nabla \boldsymbol{u} &= \omega \boldsymbol{e}_s \cdot (\boldsymbol{e}_s \partial_s \boldsymbol{u} + \boldsymbol{e}_m \partial_m \boldsymbol{u} + \boldsymbol{e}_n \partial_n \boldsymbol{u}) \\ &= \omega \partial_s \boldsymbol{u} \\ &= \omega \left(\partial_s u_s \boldsymbol{e}_s + \partial_s u_m \boldsymbol{e}_m + \partial_s u_n \boldsymbol{e}_n \right) \end{aligned} \tag{2.27}$$

where we have defined ω as the absolute value of $\boldsymbol{\omega}$.

Thus, a simplified vorticity equation may be of the form

$$\frac{\mathrm{D}\boldsymbol{\omega}}{\mathrm{D}t} = \omega \frac{\partial \boldsymbol{u}}{\partial s}, \tag{2.28}$$

or, in component notation,

$$\underbrace{\frac{\mathrm{D}\omega}{\mathrm{D}t} = \omega \frac{\partial u_s}{\partial s}}_{\text{vortex stretching}}, \qquad \underbrace{\frac{\mathrm{D}\omega_m}{\mathrm{D}t} = \omega \frac{\partial u_m}{\partial s}, \quad \frac{\mathrm{D}\omega_n}{\mathrm{D}t} = \omega \frac{\partial u_n}{\partial s}}_{\text{vortex tilting}}. \tag{2.29}$$

The first component of (2.29) means that the stretching of a vortex (positive $\partial_s u_s$) causes an increase of the vorticity, which is in accordance with the principle

of conservation of rotational momentum. The second and the third term of (2.29) cause a tilting of vortex lines (non-zero ω_m and ω_n).

Vortex stretching is one of the key mechanisms in three-dimensional turbulence. The picture here is that the strain field caused by large-scale eddies leads to stretching of smaller eddies, which results in an overall cascade of energy and enstrophy (see assignment) towards smaller scales. At the smallest scales, both energy and enstrophy are dissipated in order to balance the transport of both quantities from large to small scales. These points will be investigated in more detail below.

Figure 2.2 shows the complex structure of the vorticity field in a turbulent flow with elongated, highly distorted vortex lines as the most evident feature.

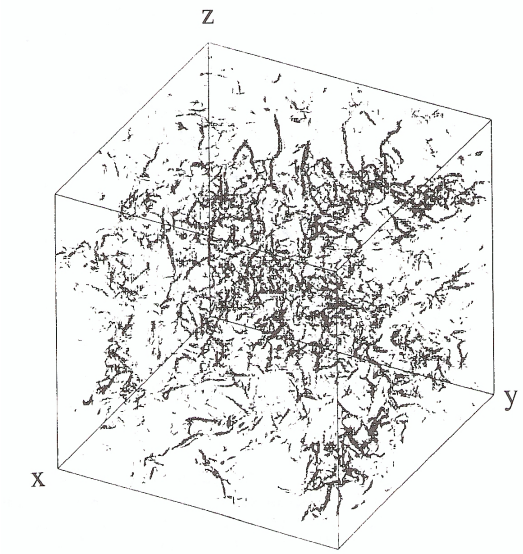

Figure 2.2: Three-dimensional view of a vorticity field in homogeneous turbulence as seen in a Direct Numerical Simulation.

2.2 Thermal energy and salinity equation

Using the Boussinesq approximation, the energy equation (first law of thermodynamics) can be expressed in terms of a transport equation for temperature. As shown in the Hydrodynamics lecture (also see Kundu and Cohen, 2008) this equation is of the form

$$\frac{\partial \theta}{\partial t} + u_j \frac{\partial \theta}{\partial x_j} - \nu^\theta \frac{\partial^2 \theta}{\partial x_j \partial x_j} = 0 \,, \tag{2.30}$$

where ν^θ denotes the molecular diffusivity of heat, which has a value of $\nu^\theta = 1.38 \cdot 10^{-7}$ m^{2}s^{-1}, slightly varying with temperature[1]

The salinity budget equation can be written as:

$$\frac{\partial S}{\partial t} + u_j \frac{\partial S}{\partial x_j} - \nu^S \frac{\partial^2 S}{\partial x_j \partial x_j} = 0 \,, \tag{2.31}$$

where ν^S is the molecular diffusivity for salinity, which has a value of $\nu^S = 1.1 \cdot 10^{-9}$ m^{2}s^{-1}.

Finally, and *equation of state* is used to related temperature and salinity (and pressure) to density, which is the dynamically relevant quantity in the Navier-Stokes equations:

$$\rho = \rho(\theta, S, p) \quad . \tag{2.32}$$

For our purpose, a linearized form of (2.32) is fully sufficient:

$$\frac{\rho}{\rho_0} = -\alpha(\theta - \theta_0) + \beta(S - S_0) \tag{2.33}$$

where α denotes the constant thermal expansion coefficient, β the constant haline contraction coefficient, and θ_0 and S_0 the constant reference temperature and salinity, respectively.

When working with geophysical flows, adiabatic compression due to the strong pressure differences at different vertical levels is known to lead to a reversible heating that has been ignored in (2.30). This effect is usually taking into account by identifying θ with the so-called *potential temperature*. This requires a different equation of state but has the advantage that the transport equation for potential temperature is to a good approximation identical to (2.30) even if compressibility effects cause substantial reversible heating. The distinction between potential and in-situ temperature is not essential for the purpose of this basic lecture on turbulence - but it should be kept in mind when working with geophysical data and models.

The concept of potential density and potential temperature, in contrast to the in-situ values, is briefly motivated here. Assume a deep *well-mixed* water column, which is understood in the sense that moving water parcels up and down does not require to perform any work against gravity. However, due to the (small) compressibility of water, both density and temperature will increase with depth (at least if θ is larger than the temperature of maximum density). These densities and temperatures are called the in-situ values obtained by local measurements (e.g. the temperature by means of a thermometer). To investigate, however, if the water column is well-mixed we have to compare *all* densities and temperatures at a *common* reference pressure that is most often associated

[1] In the ocean and the atmosphere, internal heating due to absorption of solar radiation must be considered as an inner source of heat. This process is neglected here, since it is of low significance for turbulence modeling. Furthermore, losses of kinetic energy due to internal friction, see equation (2.16), will appear as source terms in the thermal energy equation. This however is generally neglected in oceanography though it may be important in other geophysical applications.

with the surface pressure. The resulting quantities are referred to as the potential density and temperature, and take the adiabatic heating due to pressure effects into account.

Chapter 3

Flow instability and deterministic chaos

Have you ever tried to balance a billiard ball exactly on top of another (fixed) billiard ball? Although we know that this should be possible, in principle, we are unlikely to succeed as the slightest disturbance will make the ball loose balance and roll down in any direction. As the disturbance will usually be random, we will not even be able to predict in which direction that ball will eventually start rolling down. In mechanical terms, while a billiard ball sitting exactly on top of another billard ball is a perfectly valid solution of the governing mechanical equations (i.e., Newton's Laws), this solution is said to be unstable. Moreover, as the governing equations are non-linear, small differences in the initial position of the ball (or the disturbances causing the instability) will quickly amplify, strongly restricting our ability to predict the motion of the ball.

A similar situation is often found in fluid mechanics. A flow configuration may be a perfectly valid solution of the Navier-Stokes Equations — but this solution may be realized in nature only for a short duration, or not at all, because it is unstable with respect to small, random disturbances. There are numerous different types of instabilities in fluid mechanics, and their investigation forms an interesting and active area of research. Flow instabilities are especially important in the study of turbulent flows, as they generally trigger the transition from laminar to randomly fluctuating (chaotic) flow patterns, and finally to turbulence. Importantly, and similar to the example with the billiard ball above, the random nature of the disturbances initiating instabilities, and the non-linear response of the governing equations, strongly limits the predictabilty of turbulence flows. This is illustrated with the help of a famous example in the following.

3.1 Turbulence as chaotic nonlinear system

A famous example for an unstable flow configuration that shows strong sensitivity to initial conditions are the Lorenz equations for thermal convection in the atmospheric boundary layer. In thermal convection, fluid is heated from below such that irregular plumes of warm, less dense fluid rise to the top, where they cool and descend again. An example for this type of turbulent motion, called Rayleigh-Bénard convection, is shown in Figure 3.1. Fluid in a circular cylinder is heated from below with the shown patterns corresponding to a snapshot in time. The evolution is in fact chaotic in time and space, and has often been used to illustrate the chaotic nature of turbulence.

To illustrate this effect in a somewhat simpler mathematical framework, we follow the pioneering work by Lorenz. He started from the Navier-Stokes equations using the following assumptions.

1. A horizontally infinite fluid layer of depth H is heated from below;
2. The temperature profile in the unstably stratified ground state is assumed to be linear, and the density is assumed to depend linearly on temperature, i.e. the temperature gradient ΔT in the basic state is assumed to be a constant;
3. The motion is assumed to take place in the vertical x-z plane only.

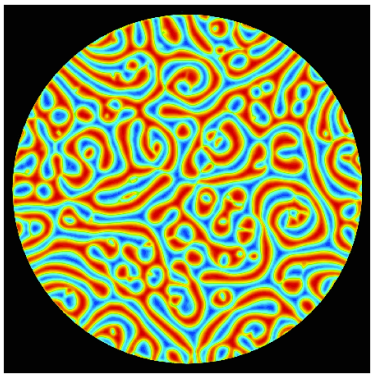

Figure 3.1: Direct numerical simulation of thermal convection in a large cylindrical cell heated from below. Shown is temperature in a horizontal cross-section with red colors corresponding to warm, rising fluid. The observed patterns evolve chaotically in time. Picture from simulations of Mark Paul, Virginia Tech.

For this situation, the equations of continuity, momentum and temperature, and the related boundary conditions (zero stress for momentum) correspond

to the Navier-Stokes equations with all gradients with respect to $x_2 = y$, and Earth rotation neglected:

$$\partial_x u + \partial_z w = 0, \tag{3.1}$$

$$\partial_t u + u\partial_x u + w\partial_z u - \nu\left(\partial_{xx} + \partial_{zz}\right) u = -\frac{1}{\rho_0}\partial_x p, \tag{3.2}$$

$$\partial_t w + u\partial_x w + w\partial_z w - \nu\left(\partial_{xx} + \partial_{zz}\right) w = -\frac{1}{\rho_0}\partial_z p - \frac{g}{\rho_0}\rho, \tag{3.3}$$

$$\partial_t \theta + u\partial_x \theta + w\partial_z \theta - \nu^\theta\left(\partial_{xx} + \partial_{zz}\right) \theta = 0, \tag{3.4}$$

with the velocity vector (u, w), the potential temperature θ, the pressure p, the potential density ρ, the reference density ρ_0, the gravitational acceleration g, the kinematic viscosity ν, and the thermal diffusivity ν^θ (Kundu and Cohen, 2008).

Introducing the streamfunction,

$$u = -\partial_z \psi, \qquad w = \partial_x \psi\ , \tag{3.5}$$

the continuity equation is automatically satisfied:

$$\partial_x u + \partial_z w = -\partial_{xz}\psi + \partial_{zx}\psi = 0 \quad . \tag{3.6}$$

Further, we define the deviation $\tilde{\theta}$ from the linear ground state as

$$\tilde{\theta} = \theta - \left(\theta_0 - z\frac{\Delta T}{H}\right), \tag{3.7}$$

with ΔT denoting the mean bottom to top temperature difference, and θ_0 the constant reference temperature. For simplicity, we assume a linear equation of state,

$$\rho = \rho_0\left(1 + \alpha\left(\theta_0 - \theta\right)\right), \tag{3.8}$$

with constant thermal expansion coefficient α.

Under these conditions, Lorenz showed that the solution of the Navier-Stokes equations is the following form:

$$\psi = X\frac{\nu^\theta\sqrt{2}(1+a^2)}{a}\sin\left(\pi a H^{-1}x\right)\sin\left(\pi H^{-1}z\right) \tag{3.9}$$

$$\tilde{\theta} = \frac{R_c\Delta T}{\pi R_a}\left[Y\sqrt{2}\cos\left(\pi a H^{-1}x\right)\sin\left(\pi H^{-1}z\right) - Z\sin\left(2\pi H^{-1}z\right)\right], \tag{3.10}$$

with the aspect ratio $a = H/B$ (with B being the length and H being the height of the convective cells). The Rayleigh number is defined according to

$$R_a = \frac{g\alpha H^3\Delta T}{\nu\nu^\theta}\ , \tag{3.11}$$

and $R_c = \pi^4 a^{-2}(1+a^2)^3$ denotes the critical Rayleigh number. X, Y and Z are scalar functions of time, obeying the following differential equation:

$$\begin{aligned} \dot{X} &= P_r(Y - X), \\ \dot{Y} &= -XZ + rX - Y, \\ \dot{Z} &= XY - bZ, \end{aligned} \tag{3.12}$$

with the Prandtl number $P_r = \nu/\nu^\theta$ (ratio of viscosity to diffusivity), the ratio of the Rayleigh number to the critical Rayleigh number, $r = R_c^{-1} R_a$, and $b = 4(1+a^2)^{-1}$. In (3.12), the dot denotes derivatives with respect to the dimensionless time $\tau = \pi^2 H^{-2}(1+a^2)\nu^\theta t$. The Lorenz equations (3.12) were published by Edward Lorenz in 1963, and layed the foundations of what is today called chaos theory. The unexpected properties of the Lorenz-equations will be investiated in the following.

It can be easily seen that the system of equations (3.12) has one trivial solution with $X = Y = Z = 0$ corresponding to $u = v = \tilde{\theta} = 0$ and two non-trivial steady-state solutions $Y = X = \pm\sqrt{b(r-1)}$, $Z = r - 1$, requiring $r > 1$. The latter represent convective cells or "rolls" in this two-dimensional view of convection. The numerical solution of (3.12) is shown in Figure 3.2 for $b = 8/3$, $P_r = 10$ and $r = 28$. These are the same values orginally chosen by Lorenz. It can be seen that the solution is oscillating around the two (unstable) states, called *attractors*, in an aperiodic, chaotic manner.

Numerical calculations of this ordinary system of equations will be task of an assignment. It will be shown that smallest perturbations in the initial values will result in a time series for X, Y and Z completely uncorrelated to the unperturbed time series from a certain point in time onwards (see Figure 3.2). This phenomenon occurs in all turbulent flows, and has been called the *butterfly effect*. Since all solutions contain minimal uncertainties, they will not converge towards any common analytical solution, for the simple reason that the latter does not exist. The reason for the chaotic behavior of the relatively simple Lorenz equations can be traced to their non-linearity, inherited from the Navier-Stokes equations.

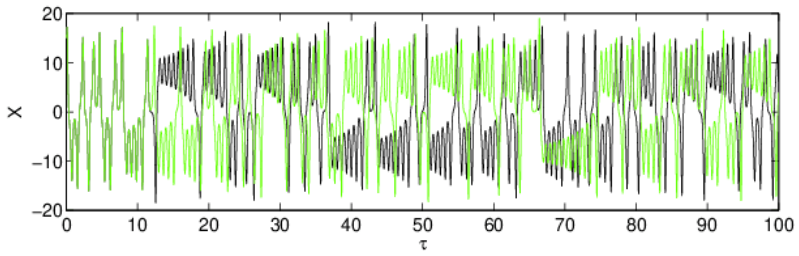

Figure 3.2: Numerical solution of (3.12) with the initial condition (X_0,Y_0,Z_0)=(15,15,15) (black curve) and (X_0,Y_0,Z_0)=(15,15,15.00001) (green curve). Note that due to the chaotic nature the solution depends on the platform, numerical accuracy, and the numerical scheme, besides the dependency on the initial condition.

Chapter 4

Statistical description

4.1 Reynolds decomposition

It was Osborn Reynolds, who, inspired by the random character of the flow in his pipe flow studies (see Section 1.3.1), suggested a decomposition of the flow into mean and fluctuating components. Analogously to the statistical concepts outlined in Section A.3, he decomposed the velocity field according to

$$u = \langle u \rangle + u' \,, \tag{4.1}$$

where the mean of the fluctuations vanishes by definition:

$$\langle u' \rangle = 0 \quad . \tag{4.2}$$

Using the properties of the probability density function $f(V)$ discussed in Section A.3, it is easy to show that the mean obeys the following fundamental relations for the two random variables u and v, and the constant λ:

1. Linearity:
$$\langle u + \lambda v \rangle = \langle u \rangle + \lambda \langle v \rangle \tag{4.3}$$

2. Derivatives and averages commute:
$$\langle \partial_x u \rangle = \partial_x \langle u \rangle \,, \quad \langle \partial_t u \rangle = \partial_t \langle u \rangle \tag{4.4}$$

3. Double averages:
$$\langle \langle u \rangle \rangle = \langle u \rangle \tag{4.5}$$

4. Product average:
$$\langle u \langle v \rangle \rangle = \langle u \rangle \langle v \rangle \tag{4.6}$$

As discussed in Section A.3, all single-point statistical parameters of the velocity field can be computed if the probability density distribution $f(V)$ is

known. E.g., the mean velocity $\langle u \rangle$ was shown to simply follow from the first moment of the PDF:

$$\langle u \rangle = \int_{-\infty}^{\infty} V f(V) \mathrm{d}V \quad .$$

In most cases, however, $f(V)$ is not known and has to be estimated in some way. To this end let's consider a fluid mechanics experiment that is repeated N times under identical conditions, C. In his excellent book on turbulent flows, Pope (2000) remarks about the random nature of the results:

> An example is the flow of pure water at 20°C through a smooth straight pipe. It should be appreciated that the conditions, C, thus defined are incomplete: in practise there are, inevitably, perturbations from these nominal conditions. There can be perturbations in boundary conditions, for example, through vibrations of the apparatus, or from the detailed finish of nominally smooth surfaces. There can be perturbations in fluid properties caused by small inhomogeneities in temperature or by the presence of impurities, and there can be perturbations in the initial state of the flow. With care and effort, these perturbations can be reduced, but they cannot be eliminated. Consequently, the nominal conditions, C, are incomplete, and hence do not uniquely determine the evolution of the turbulent flow.

This finding is qualitatively similar to our observation that the solutions of the Lorenz equations discussed in Section 3.1 are extremely sensitive even to the smallest variations in the initial conditions. Thus, at a certain time t and at a certain position $\boldsymbol{x}$ each realization of the experiment will yield a random value $u^{(k)}$ for the velocity, where k is the index of the realization. If the experiment is repeated N times, we expect that the relation

$$\langle u \rangle_N \approx \frac{1}{N} \sum_{k=1}^{N} u^{(k)} \tag{4.7}$$

provides an *estimate* of the true mean value $\langle u \rangle$. However, only in the limit $N \to \infty$, this estimate will coincide with the true mean.

While in laboratory settings and numerical simulations of the Navier-Stokes equations, estimators of the type (4.7) are indeed sometimes used to derive statistical parameters, repeating the "experiment" is evidently not an option in real-world geophysical flows. In this case, different types of *filtering procedures* are applied to separate the mean from the fluctuating components. Except under very special conditions, however, none of these methods is exactly consistent with the ensemble averaging procedure described above, and they should be used with great caution. Some examples of the problems involved in filtering are described in the following.

The two most frequently used filtering procedures are a box-type time filter,

$$\langle u(\boldsymbol{x},t)\rangle_T = \frac{1}{T}\int_{t-T/2}^{t+T/2} u(\boldsymbol{x},\tau)\,\mathrm{d}\tau\ , \tag{4.8}$$

where T is the fixed filter width, or the spatial equivalent,

$$\langle u(\boldsymbol{x},t)\rangle_V = \frac{1}{V}\int_V u(\boldsymbol{\xi},t)\,\mathrm{d}\boldsymbol{\xi}\ , \tag{4.9}$$

where V denotes the filtering volume, and $\boldsymbol{\xi}$ the integration variable centered around the local position $\boldsymbol{x}$.

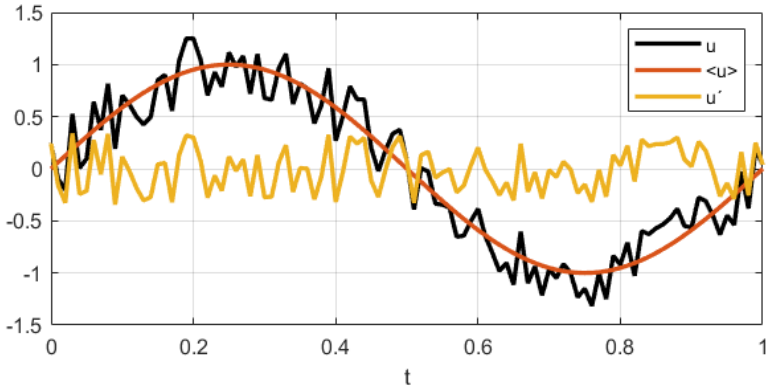

Figure 4.1: Synthetically generated times series of the dimensionless random variable $u(t)$, consisting of a mean sinusoidal variation, $\langle u\rangle$, superimposed by random fluctuations, u'.

In order to demonstrate the weaknesss of the above averaging procedures, an example of a time series of synthetically generated data is considered (Figure 4.1). This time series consists of a sine wave with amplitude 1, superimposed with some random noise with a standard deviation of 0.1. Here, we want to decompose the time series of u into a mean component and a fluctuating component by time filtering according to (4.8), not using our a-priori knowledge about the composition of the time series. This is shown in Figure 4.2a for two different averaging intervals. For the smaller averaging window ($T = 0.05$), many of the fluctuations are still visible in the averaged fields. Moreover, Figure 4.2b shows that the time average of the fluctuations does not vanish as it should according to (4.2), suggesting that time filtering is not consistent with the basic properties of the averaging operator. If the averaging windows is increased ($T = 0.2$), these fluctutions become smaller — but only at the price that the original sinussoidal signal that we wanted to recover looses more than

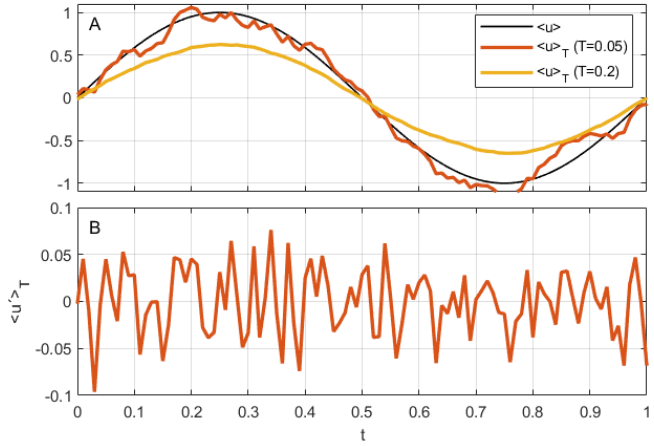

Figure 4.2: The effect of time averaging: (a) true mean velocity $\langle u \rangle$ and time filtered velocity $\langle u \rangle_T$ computed from (4.8) for different averaging windows T, and (b) time average $\langle u' \rangle_T$ of the velocity fluctuations $u' = u - \langle u \rangle_T$ for an averaging window of $T = 0.05$.

30% of its amplitude! It is easy to show that even for this simple time series, there is no choice of T that yields the correct separation of mean and fluctating parts.

For a demonstration of the ensemble averaging concept using the estimator in (4.7), we again use the synthetically generated time series introduced above. Each relization k now consists of the same sine curve, representing the mean, superimposed with random fluctuations that are individually different but statistically equivalent (i.e. they have the same PDF). The estimated averages for $N = 10$ and $N = 1000$ realizations are shown in Figure 4.3. For smaller N fluctuations are still visible, but for larger N, the ensemble average clearly converges to $\langle u \rangle$ (Figure 4.3a), and the average of the fluctuations converges to zero (Figure 4.3b).

Note, however, that for *statistically stationary* flows (flows in which the PDF does not depend on time), time filtered quantities do converge to the true mean, provided the filter width is much larger than the autocorrelation time scale. Similarly, for *statistically homogeneous* flows (flows in which the PDF does not depend on space) spatial filtering can be used to represent the mean value, provided the filter width is much larger than spatial autocorrelation scale. Stationary and homogeneous random processes, in which this equivalence holds, are called *ergodic*. The conditions for the validity of ergodicity assumption are, however, often violated in real-world flows, which may become particularly

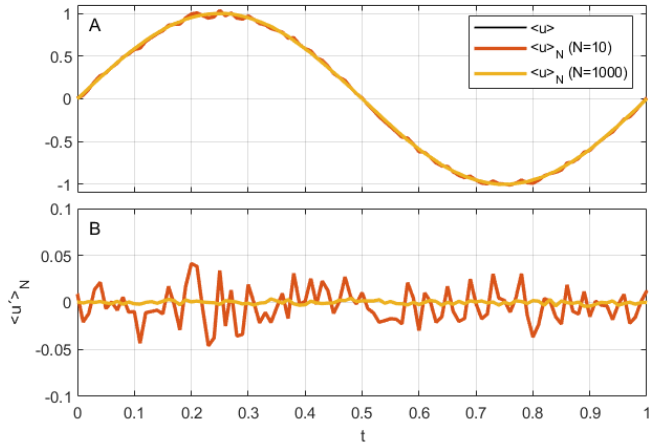

Figure 4.3: The effect of ensemble averaging: (a) true mean velocity $\langle u \rangle$ and ensemble averages $\langle u \rangle_N$ computed from (4.7) for two different values of N, and (b) ensemble average $\langle u' \rangle_N$ of the velocity fluctuations $u' = u - \langle u \rangle_N$ for different values of N (line colors correspond to panel a).

problematic when temporal (or spatial) variations in the mean flow have similar scales as the turbulent fluctuations.

4.2 The Reynold's equations

A set of equations for the mean velocity $\langle u \rangle$ can be obtained by inserting the Reynolds decomposition (4.1) into the equations describing the instantaneous motions, and subsequent averaging. E.g., inserting (4.1) into the continuity equation (2.2) yields

$$\partial_i \left(\bar{u}_i + u_i' \right) = 0 \,, \tag{4.10}$$

where here and in the following we use the short-hand notation $\bar{u}_i \equiv \langle u_i \rangle$ for the mean. Averaging this equation, taking into account (4.4) and the fact that the mean of the fluctuations vanishes according to (4.2), we obtain

$$\partial_i \bar{u}_i = 0 \,, \tag{4.11}$$

indicating that also the mean flow is divergence-free. Substracting (4.11) from (4.10) shows that the same is true also for the fluctations:

$$\partial_i u_i' = 0 \quad . \tag{4.12}$$

In a similar way, a transport equation for the mean momentum may be obtained from inserting, in a first step, the Reynolds decomposition (4.1) into the Navier-Stokes equations in (2.6):

$$\begin{aligned} &\partial_t \left(\bar{u}_i + u_i' \right) + \bar{u}_j \partial_j \bar{u}_i + \bar{u}_j \partial_j u_i' + u_j' \partial_j \bar{u}_i + u_j' \partial_j u_i' - \nu \partial_{jj} \left(\bar{u}_i + u_i' \right) + 2 \varepsilon_{ijl} \Omega_j \left(\bar{u}_l + u_l' \right) \\ &\quad = - \frac{\partial_i \left(\bar{p} + p' \right)}{\rho_0} + \frac{g_i}{\rho_0} \left(\bar{\rho} + \rho' \right) \quad . \end{aligned} \tag{4.13}$$

Averaging this equation, using the fundamental properties of the mean compiled in (4.3)-(4.6) and the fact that the mean of fluctuations vanishes by definition according to (4.2), we obtain the following *Reynolds equations* describing the evolution of mean momentum:

$$\partial_t \bar{u}_i + \bar{u}_j \partial_j \bar{u}_i + \langle u_j' \partial_j u_i' \rangle - \nu \partial_{jj} \bar{u}_i + 2 \varepsilon_{ijl} \Omega_j \bar{u}_l = - \frac{\partial_i \bar{p}}{\rho_0} + \frac{g_i}{\rho_0} \bar{\rho} \quad . \tag{4.14}$$

Using the continuity equation in (4.11) and (4.12), this equation can be re-written as

$$\partial_t \bar{u}_i + \partial_j \left(\bar{u}_i \bar{u}_j + \langle u_i' u_j' \rangle - \nu \partial_j \bar{u}_i \right) + 2 \varepsilon_{ijl} \Omega_j \bar{u}_l = - \frac{\partial_i \bar{p}}{\rho_0} + \frac{g_i}{\rho_0} \bar{\rho} \,, \tag{4.15}$$

which is identical to the original Navier-Stokes equations (2.6), except for two important differences: instantaneous quantities have been replaced by mean quantities, and the term $\left\langle u_i' u_j' \right\rangle$ has appeared in the bracketed expression on

the left hand side. This term represents the momentum flux supported by the turbulent motions, and appears in addition to the mean advective flux (first term in brackets) and the diffusive flux (third term). Stastically, $\langle u_i' u_j' \rangle$ represent the correlation between different velocity components. Since a momentum flux is physically equivalent to a stress, the second-order tensor $\langle u_i' u_j' \rangle$ is often referred to as the *Reynolds Stress tensor*.

Analogously, the decomposition of the temperature into mean and fluctuating parts $\theta = \bar{\theta} + \theta'$ can be inserted into (2.30). Averaging results in a transport equation for the mean temperature:

$$\partial_t \bar{\theta} + \partial_i \left(\bar{u}_i \bar{\theta} + \langle u_i' \theta' \rangle - \nu^\theta \partial_i \bar{\theta} \right) = 0 \,, \tag{4.16}$$

where again we have used (4.3)-(4.6), as well as (4.11) and (4.12). Similar to the Reynolds stress appearing in (4.15), also in (4.16) a new term has appeared: the correlation $\langle u_i' \theta' \rangle$ representing the turbulent heat flux. As in (4.15), this term providing an important (often dominant) additional transport mechanism for heat besides the mean advective and diffusive terms.

4.3 Mean and turbulent kinetic energy

In the previous chapter, we have seen that a transport equation of the form (2.16) can be derived for the kinetic energy of the flow as defined in (2.15). As any other fluctuating quantity, also the total kinetic energy can be decomposed into mean and fluctuating parts. The mean kinetic energy is obtained from inserting the Reynolds-decomposition (4.1) into (2.15), and averaging:

$$\langle E \rangle = \frac{1}{2} \langle u_i u_i \rangle = \frac{1}{2} \bar{u}_i \bar{u}_i + \frac{1}{2} \langle u_i' u_i' \rangle \quad . \tag{4.17}$$

The first part is referred to as the *kinetic energy of the mean flow*,

$$\bar{E} = \frac{1}{2} \bar{u}_i \bar{u}_i \,, \tag{4.18}$$

where it should be noted that, contrary to our usual notation, $\bar{E} \neq \langle E \rangle$. The second contribution to the mean energy is the *turbulent kinetic energy* defined as

$$k = \frac{1}{2} \langle u_i' u_i' \rangle \quad . \tag{4.19}$$

Some interesting insights can be gained by investigating the equations governing the evolution of $\bar{E}$ and k. To this end, similar to the derivation of (2.16), we start from the general momentum budget in (4.20). Taking the mean of this equation yields

$$\partial_t \bar{u}_i + \partial_j \left(\bar{u}_i \bar{u}_j + \langle u_i' u_j' \rangle - \frac{1}{\rho_0} \bar{T}_{ij} \right) + 2 \varepsilon_{ijl} \Omega_j \bar{u}_l = \frac{g_i}{\rho_0} \bar{\rho} \,, \tag{4.20}$$

which is completely analogous to (4.15) but more general since we haven't made any assumptions about the material properties about the fluid. Using (4.20) as

the starting point for the following analysis, it is straightforward to identify the physical meaning of the terms in the equation for the mean energy. The latter follows from the inner product of (4.20) with $\bar{u}_i$:

$$\partial_t \bar{E} + \partial_j \left(\bar{u}_j \bar{E} + \bar{u}_i \langle u_i' u_j' \rangle - \frac{\bar{u}_i \bar{T}_{ij}}{\rho_0} \right) = \langle u_i' u_j' \rangle \bar{S}_{ij} - \frac{g}{\rho_0} \bar{u}_3 \bar{\rho} - \frac{1}{\rho_0} \bar{T}_{ij} \bar{S}_{ij} \ , \qquad (4.21)$$

where $\bar{S}_{ij}$ denotes the mean rate of the rate strain tensor S_{ij} defined in (2.4). The left hand side of (4.21) describes the balance between the local rate of change and the three types of transport terms: (a) advection with the mean flow, (b) transport by turbulent motions, and (c) transport by mean stress. The terms on the right hand side desribe the work done (a) against the turbulent Reynolds stress, (b) against gravity, and (c) against the mean stress. Note that the rotation terms have no direct effect in the energy budget. Inserting the mean of the Cauchy-Poisson law (2.3) into (4.21) finally results in the energy equation for the mean flow of a viscous Newtonian Boussinsq-fluid:

$$\begin{aligned} \partial_t \bar{E} \quad &+ \quad \partial_j \left(\bar{u}_j \bar{E} + \bar{u}_i \langle u_i' u_j' \rangle - 2\nu \bar{u}_i \bar{S}_{ij} + \frac{\bar{u}_j \bar{p}}{\rho_0} \right) \\ &= \quad \langle u_i' u_j' \rangle \bar{S}_{ij} - \frac{g}{\rho_0} \bar{u}_3 \bar{\rho} - 2\nu \bar{S}_{ij} \bar{S}_{ij} \quad . \end{aligned} \qquad (4.22)$$

Here, the stress transport appearing on the left hand side of (4.21) results in two different contributions: the viscous transport and the pressure transport. The work against the mean viscous stress on the right hand side always provides a sink of energy, and represents the conversion of kinetic energy of the mean flow into internal energy via viscous dissipation. In flows with high Reynolds number, this term is usually very small compared to the others.

Using a procedure similar to that leading to (4.22), also an equation for the turbulent kinetic energy (TKE) can be derived. To this end, we start again from (2.1), take the inner product with $\boldsymbol{u}'$, and average. After inserting the material law (2.3) for Newtonian fluids, and some re-arrangements (see assignment), an equation for the TKE can be derived:

$$\begin{aligned} \partial_t k \quad &+ \quad \partial_j \left(\bar{u}_j k + \frac{1}{2} \langle u_i' u_i' u_j' \rangle - 2\nu \langle u_i' S_{ij}' \rangle + \frac{\langle u_j' p' \rangle}{\rho_0} \right) \\ &= \quad -\langle u_i' u_j' \rangle \bar{S}_{ij} - \frac{g}{\rho_0} \langle u_3' \rho' \rangle - 2\nu \langle S_{ij}' S_{ij}' \rangle \quad . \end{aligned} \qquad (4.23)$$

The transport terms on the left hand side are, in their order of appearence: transport of TKE by the mean flow, transport by turbulent motions, viscous transport, and pressure transport. The first term on the right hand (work against the Reynolds stress) is identical to a term appearing on the right hand side of (4.22), however, with opposite sign. From this, we conclude that this *shear-production* term represents the conversion from mean-flow energy to TKE, and vice-versa. The sign of this term is unkown but in most turbulent flows

energy cascades from the mean flow towards turbulence, apart from rare exceptions. The second term corresponds to the *turbulent buoyancy flux*, which, here, has a second interpretation as the conversion between TKE and potential energy. The final term is the *rate of dissipation* of TKE into internal energy, or, in other words, the work performed by the small-scale turbulent motions against viscous forces. This term is of crucial importance in essentially all turbulent flows.

4.4 Temperature variance and potential energy

In a thermally stratified fluid, the temperature variance $\langle \theta'^2 \rangle$ is a useful measure for the magnitude of temperature fluctuations in the flow. To understand the mechanisms by which such temperature fluctuations are generated, transported, and destroyed, it is instructive to derive a transport equation for $\langle \theta'^2 \rangle$. To this end, (2.30) describing the evolution of the instantaneous temperature field is multiplied by θ', and subsequently averaged, resulting in (see assignments):

$$\begin{aligned} \partial_t \langle \theta'^2 \rangle + \partial_j \left(\bar{u}_j \langle \theta'^2 \rangle + \langle u_j' \theta'^2 \rangle - \nu^\theta \partial_j \langle \theta'^2 \rangle \right) = \\ \underbrace{- 2 \langle u_j' \theta' \rangle \partial_j \bar{\theta}}_{P_\theta} \underbrace{- 2 \nu^\theta \langle \partial_j \theta' \partial_j \theta' \rangle}_{\chi_\theta} \quad . \end{aligned} \tag{4.24}$$

On the left hand side of (4.24), we find three transport terms representing the effect of mean-flow advection, transport by turbulent motions, and transport by molecular heat conduction. On the right hand side, P_θ is the production of temperature variance due to mean temperature gradients. Similar to the shear-production term in the TKE budget (4.23), this term provides a source of temperature variance in most cases also this property cannot be mathematically proven in general. The second term χ_θ denotes the dissipation of temperature variance $\langle \theta'^2 \rangle$. By definition, this term provides a sink under all conditions such that P_θ remains as the only possible source term. An equation similar to (4.24) for the salinity variance can be derived from (2.31).

It is important to note that both temperature and salinity fluctuations are related to density fluctuations via the equation of state (2.32). This implies that, apart from the TKE, turbulent fluctuations also support *potential energy* as the second important form of mechanical energy in stratified turbulent flows. For the special case of stratified homogenous turbulence, it is shown in the assignments how an equation for the turbulent potential energy can be derived from (4.24).

4.5 The second moment equations

In addition to the transport equation (4.23) for the TKE, $k = \langle u_i' u_i' \rangle / 2$, similar equations can be derived also for mixed terms of the form $\langle u_i' u_j' \rangle$. These sec-

ond statistical moments represent the correlations between different fluctuating velocity components, i.e. the turbulent momentum flux or the Reynolds stress.

The derivation starts from the general momentum budget in (2.1). The equation for u_i is multiplied by u_j', and added to the equation for u_j multiplied by u_i'. The result is averaged. Taking the rate term as an example, this yields

$$\left\langle u_j' \partial_t (\bar{u}_i + u_i') + u_i' \partial_t (\bar{u}_j + u_j') \right\rangle = \partial_t \left\langle u_i' u_j' \right\rangle , \tag{4.25}$$

where we have used the averaging rules in (4.3) – (4.6). The other terms can be found in a fashion similar to that used in deriving (4.23). After inserting the Cauchy-Poisson law (2.3) for viscous fluids, it can be shown that the resulting transport equation is of the form:

$$\begin{aligned}
&\partial_t \langle u_i' u_j' \rangle + \partial_l \left(\bar{u}_l \langle u_i' u_j' \rangle + \left\langle u_l' u_i' u_j' \right\rangle - 2\nu \left\langle u_j' S_{il}' \right\rangle - 2\nu \left\langle u_i' S_{jl}' \right\rangle + \langle u_i' p' \rangle \delta_{jl} + \left\langle u_j' p' \right\rangle \delta_{il} \right) \\
&\quad = \underbrace{-\partial_l \bar{u}_i \langle u_l' u_j' \rangle - \partial_l \bar{u}_j \langle u_l' u_i' \rangle}_{P_{ij}} \underbrace{- 2\Omega_l (\varepsilon_{ilk} \langle u_j' u_k' \rangle + \varepsilon_{jlk} \langle u_i' u_k' \rangle)}_{\Omega_{ij}} \\
&\qquad + \underbrace{\frac{g_i}{\rho_0} \langle u_j' \rho' \rangle + \frac{g_j}{\rho_0} \langle u_i' \rho' \rangle}_{B_{ij}} + \underbrace{\frac{2}{\rho_0} \left\langle S_{ij}' p' \right\rangle}_{\Pi_{ij}} \underbrace{- 2\nu \left\langle S_{il}' S_{jl}' \right\rangle}_{\varepsilon_{ij}},
\end{aligned} \tag{4.26}$$

The terms in brackets on the left hand side are transport terms, similar in character to those found in (4.23). The terms on the right hand side are grouped together such that P_{ij} is the shear production, Ω_{ij} redistribution of energy among different components of the Reynolds stress tensor due to rotation, B_{ij} the buoyancy production, Π_{ij} the pressure-strain correlation, and ε_{ij} the viscous redistribution and dissipation of the Reynolds stress. Note that the contraction of (4.26) yields the TKE budget (4.23).

Similarly, a transport equation for the heat flux $\langle u_i' \theta' \rangle$ can be derived. To this end, we multiply (2.30) with u_i', and add the result to the product of θ' and the momentum budget for u_i' in (2.1). After averaging, this results in a second-moment transport equation of the form

$$\begin{aligned}
&\frac{\partial \langle u_i' \theta' \rangle}{\partial t} + \frac{\partial}{\partial x_j} \left(\bar{u}_j \langle u_i' \theta' \rangle + \langle u_i' u_j' \theta' \rangle - \nu \langle \theta' \frac{\partial u_i'}{\partial x_j} \rangle - \nu_\theta \langle u_i' \frac{\partial \theta'}{\partial x_j} \rangle + \frac{\langle p' u_i' \rangle}{\rho_0} \right) \\
&\quad = \underbrace{- \langle u_i' u_j' \rangle \frac{\partial \bar{\theta}}{\partial x_j} - \langle u_j' \theta' \rangle \frac{\partial \bar{u}_i}{\partial x_j}}_{P_{i\theta}} \underbrace{- \frac{g}{\rho_0} \delta_{i3} \langle \rho'^2 \rangle}_{G_{i\theta}} \underbrace{- 2\varepsilon_{ijl} \Omega_j \langle u_l' \theta' \rangle}_{\Omega_{i\theta}} \\
&\qquad + \underbrace{\frac{1}{\rho_0} \left\langle p' \frac{\partial \theta'}{\partial x_i} \right\rangle}_{\Pi_{i\theta}} \underbrace{- (\nu + \nu_\theta) \left\langle \frac{\partial u_i'}{\partial x_l} \frac{\partial \theta'}{\partial x_l} \right\rangle}_{\varepsilon_{i\theta}}
\end{aligned} \tag{4.27}$$

Here, $P_{i\theta}$ is the production of heat fluxes due to the presence of mean-flow gradients, $\Omega_{i\theta}$ denotes the effect of system rotation, $B_{i\theta}$ the buoyancy production,

$\Pi_{i\theta}$ the pressure-scrambling term, and $\varepsilon_{i\theta}$ the molecular effects.

It is important to note that new unknowns have emerged in the equations, namely the third moments $\langle u_i' u_j' u_k' \rangle$, $\langle u_i' u_j' \theta' \rangle$ and $\langle u_i' \theta'^2 \rangle$ and the pressure-strain correlators Π_{ij} and $\Pi_{i\theta}$. Also for these correlators, transport equations can be derived from the momentum budget (2.1), and the transport equations for salinity (2.31) and temperature (2.30). However, these include fourth moments, and other unkown pressure terms such that a closed set of equations can never be obtained. This illustrates the well-known closure problem of statistical turbulence. A closed form of the equations can only be found by relating these higher moments to known statistical quantities. While until now, we have only used mathematical manipulations of the equations, this step requires physical modeling assumptions that are not trivial. We will come back to this problem later during this lecture.

Chapter 5

Spectra theory of homogeneous turbulence

5.1 Velocity correlations and energy spectra

The autocorrelation of a fluctuating variable $u'(t)$ at two times t_1 and t_2 is defined as

$$R(t_1, t_2) = \langle u'(t_1) u'(t_2) \rangle \quad . \tag{5.1}$$

In the case of a statistically stationary process, the autocorrelation only depends on $\tau = t_2 - t_1$, and, instead of (5.1), the autocorrelation is defined more compactly as

$$R(\tau) = \langle u'(t) u'(t+\tau) \rangle \quad . \tag{5.2}$$

Normalizing by the variance yields the correlation coefficient

$$r(\tau) = \frac{\langle u'(t) u'(t+\tau) \rangle}{\left\langle u'^2 \right\rangle} \quad . \tag{5.3}$$

For any $u'(t)$, it can be shown that

$$|\langle u'(t_1) u'(t_2) \rangle| \leq \left\langle u'^2(t_1) \right\rangle^{1/2} \left\langle u'^2(t_2) \right\rangle^{1/2}, \tag{5.4}$$

which is usually referred to Schwartz' inequality. This inequality implies that $|r| \leq 1$ for all τ. Figure 5.1 demonstrates how the autocorrelation of a statistically stationary time series can be calculated. A typical autocorrelation plot is shown in figure 5.2. For the time lag $\tau = 0$, the autocorrelation is trivially unity, and it decays with increasing time lag. For the limit $\tau \to \infty$, we have $r \to 0$ because the turbulent eddies that determine the correlation only have finite duration. This allows for the definition of an integral time scale $\mathcal{T}$ of turbulence:

$$\mathcal{T} = \int_0^\infty r(\tau) \, \mathrm{d}\tau \, , \tag{5.5}$$

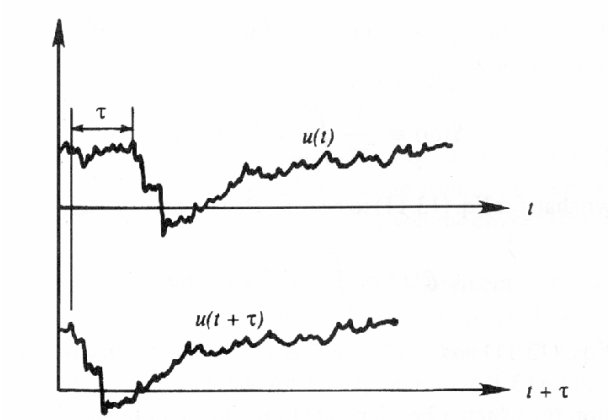

Figure 5.1: Method of calculating the autocorrelation $R(\tau) = \langle u'(t)u'(t+\tau)\rangle$. This figure has been taken from Kundu and Cohen (2008).

see figure 5.2 for a graphical demonstration. $\mathcal{T}$ represents the time over which the process $u'(t)$ is highly correlated to itself.

Let now $u_i'(t)$ denote the fluctuating part of the velocity at a point. In this case, the combination of all possible correlations can be written compactly in tensor form as

$$R_{ij}(\tau) = \left\langle u_i'(t)u_j'(t+\tau)\right\rangle , \tag{5.6}$$

which is real and symmetric in τ.

For $\tau = 0$ we obtain the one-point correlation which is recognized as the Reynolds stress tensor $R_{ij}(0) = \left\langle u_i'u_j'\right\rangle$ defined in Section 4.2.

Let $\Phi_{ij}(\omega)$ denote the Fourier transform of the correlation function $R_{ij}(\tau)$:

$$\Phi_{ij}(\omega) = \frac{1}{2\pi}\int_{-\infty}^{\infty} e^{-i\omega\tau}R_{ij}(\tau)\,\mathrm{d}\tau \tag{5.7}$$

where ω is the frequency of the oberved motions. The inverse Fourier transform is then defined as

$$R_{ij}(\tau) = \int_{-\infty}^{\infty} e^{i\omega\tau}\Phi_{ij}(\omega)\,\mathrm{d}\omega , \tag{5.8}$$

such that (5.7) and (5.8) form a *Fourier transform pair*.

For $\tau = 0$ and $i = j$, we immediately see from (5.8) that

$$\langle u_i'u_i'\rangle = \int_{-\infty}^{\infty}\Phi_{ii}(\omega)\,\mathrm{d}\omega \quad . \tag{5.9}$$

Since $R_{ii}(\tau)$ is real and symmetric, it is easy to show from (5.7) that also $\Phi_{ii}(\omega)$ is real and symmetric. Therefore, (5.9) can be written as

$$k = \int_{0}^{\infty}\Phi_{ii}(\omega)\,\mathrm{d}\omega \tag{5.10}$$

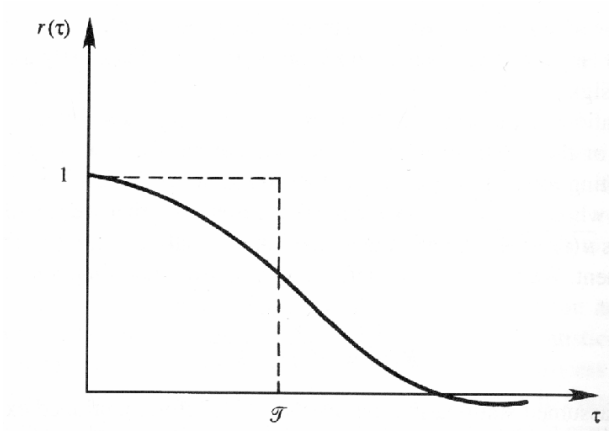

Figure 5.2: Autocorrelation function $r(\tau)$ and the integral time scale $\mathcal{T}$. This figure has been taken from Kundu and Cohen (2008).

with the turbulent kinetic energy k defined in (4.19). The physical interpretation of (5.10) is that $\Phi_{ii}(\omega)\,\mathrm{d}\omega$ represent the turbulent kinetic energy in a frequency band $\mathrm{d}\omega$ centered around ω. Further, we note that

$$\Phi_{ii}(0) = \frac{1}{2\pi}\int_{-\infty}^{\infty} R_{ii}(\tau)\,\mathrm{d}\tau = \frac{\left\langle u_j' u_j' \right\rangle}{\pi}\int_0^{\infty} r_{ii}(\tau)\,\mathrm{d}\tau = \frac{\left\langle u_j' u_j' \right\rangle}{\pi}\mathcal{T} \tag{5.11}$$

which shows that the spectrum at zero frequency is proportional to the integral time scale.

5.1.1 The energy spectrum

So far, we have only considered correlations in time. However, correlations in space can be treated in an analogue way. Let $\boldsymbol{x}_0$ and $\boldsymbol{x}_0 + \boldsymbol{x}$ be two points in the three-dimensional Cartesian space. Then the spatial cross correlation of a function $u_i'(\boldsymbol{x}, t)$ can be formulated as

$$R_{ij}(\boldsymbol{x}, \boldsymbol{r}) = \left\langle u_i'(\boldsymbol{x}, t) u_j'(\boldsymbol{x} + \boldsymbol{r}, t) \right\rangle , \tag{5.12}$$

where $\boldsymbol{r}$ denotes the spatial separation between the two points considered.

Assuming homogeneous turbulence (analogous to our assumption of stationary turbulence above), the energy spectrum tensor $\Phi_{ij}(\boldsymbol{K})$ with the wave number vector $\boldsymbol{K}$ can be formulated in the same way as in (5.7):

$$\Phi_{ij}(\boldsymbol{K}) = \frac{1}{(2\pi)^3}\iiint_{-\infty}^{\infty} e^{-i\boldsymbol{K}\cdot\boldsymbol{r}} R_{ij}(\boldsymbol{r})\,\mathrm{d}\boldsymbol{r} , \tag{5.13}$$

with the inverse relation

$$R_{ij}(\boldsymbol{r}) = \iiint_{-\infty}^{\infty} e^{i\boldsymbol{K}\cdot\boldsymbol{r}} \Phi_{ij}(\boldsymbol{K})\,\mathrm{d}\boldsymbol{K} \quad . \tag{5.14}$$

For $i = j$ and $\boldsymbol{r} = \boldsymbol{0}$ we obtain

$$R_{ii}(\boldsymbol{0}) = \langle u_i' u_i' \rangle = \iiint_{-\infty}^{\infty} \Phi_{ii}(\boldsymbol{K}) \, \mathrm{d}\boldsymbol{K}. \tag{5.15}$$

For simplicity, the information about the directional information in $\boldsymbol{K}$ often removed, considering only the length of the wave number vector, $K = \left(K_i^2\right)^{1/2}$ instead. The corresponding expression is derived by integrating (5.15) over the surface of a sphere $\mathcal{S}(K)$ with radius K:

$$k = \frac{1}{2}\langle u_i' u_i' \rangle = \iiint_{-\infty}^{\infty} \frac{1}{2}\Phi_{ii}(\boldsymbol{K}) \, d\boldsymbol{K} = \int_0^{\infty} \oint_{\mathcal{S}(K)} \frac{1}{2}\Phi_{ii}(\boldsymbol{K}) \, \mathrm{d}\mathcal{S}(K) \, \mathrm{d}K \quad . \tag{5.16}$$

Defining

$$E(K) = \oint_{\mathcal{S}(K)} \frac{1}{2}\Phi_{ii}(\boldsymbol{K}) \mathrm{d}S \, , \tag{5.17}$$

we can thus re-write (5.16) in the form

$$k = \frac{1}{2}\langle u_i' u_i' \rangle = \int_0^{\infty} E(K) \, \mathrm{d}K \, , \tag{5.18}$$

revealing the *energy spectrum* $E(K)$ as the energy density per wave number.

5.1.2 The dissipation spectrum

As discussed above in the context of (4.23), the turbulence dissipation rate $\varepsilon = 2\nu\langle S_{ij}' S_{ij}' \rangle$ represents the irreversible conversion of TKE into internal energy, which is of crucial importance for the energetics of any turbulent flow. In homogenous turbulence, the expression for ε can be written in the somewhat simpler form (see assignments):

$$\varepsilon = \nu \left\langle \frac{\partial u_i'}{\partial x_j} \frac{\partial u_i'}{\partial x_j} \right\rangle \, , \tag{5.19}$$

which will form the starting point for the following discussion. Analogously to the energy spectrum defined in (5.18), we can also define a dissipation spectrum,

$$\varepsilon = \nu \left\langle \frac{\partial u_i'}{\partial x_j} \frac{\partial u_i'}{\partial x_j} \right\rangle = \int_0^{\infty} D(K) \, \mathrm{d}K \quad . \tag{5.20}$$

While $E(K)$ contains information about the energy-containing scales, the dissipation spectrum $D(K)$ characterizes the scales at which energy is dissipated. As both quantities are derived from the same velocity field, we expect that they are related.

To find this relationship, we start from the observation that

$$\frac{\partial}{\partial x_l} \left\langle u_i'(\boldsymbol{x}) \frac{\partial u_j'(\boldsymbol{x} + \boldsymbol{r})}{\partial x_m} \right\rangle = 0 \, , \tag{5.21}$$

for homogeneous turbulence. Using the product rule of differentation, (5.21) can be re-written in the following form:

$$\begin{aligned}\left\langle \frac{\partial u_i'(\boldsymbol{x})}{\partial x_l}\frac{\partial u_j'(\boldsymbol{x}+\boldsymbol{r})}{\partial x_m}\right\rangle &= -\left\langle u_i'(\boldsymbol{x})\frac{\partial^2 u_j'(\boldsymbol{x}+\boldsymbol{r})}{\partial x_l \partial x_m}\right\rangle \\ &= -\left\langle u_i'(\boldsymbol{x})\frac{\partial^2 u_j'(\boldsymbol{x}+\boldsymbol{r})}{\partial r_l \partial r_m}\right\rangle \\ &= -\frac{\partial^2 \left\langle u_i'(\boldsymbol{x})u_j'(\boldsymbol{x}+\boldsymbol{r})\right\rangle}{\partial r_l \partial r_m}\ ,\end{aligned} \tag{5.22}$$

where the quantity appearing in the numerator in the last line is recognized as the correlation tensor R_{ij} defined in (5.12). Using the Fourier representation of R_{ij} in (5.14), we can therefore re-arrange (5.22) in the following way:

$$\begin{aligned}\left\langle \frac{\partial u_i'(\boldsymbol{x})}{\partial x_l}\frac{\partial u_j'(\boldsymbol{x}+\boldsymbol{r})}{\partial x_m}\right\rangle &= -\frac{\partial^2 R_{ij}(\boldsymbol{r})}{\partial r_l \partial r_m} \\ &= -\frac{\partial^2}{\partial r_l \partial r_m}\iiint_{-\infty}^{\infty} e^{i\boldsymbol{K}\cdot\boldsymbol{r}}\Phi_{ij}(\boldsymbol{K})\,\mathrm{d}\boldsymbol{K} \\ &= \iiint_{-\infty}^{\infty} K_l K_m e^{i\boldsymbol{K}\cdot\boldsymbol{r}}\Phi_{ij}(\boldsymbol{K})\,\mathrm{d}\boldsymbol{K}\quad .\end{aligned} \tag{5.23}$$

Setting $i = j$ and $l = m$, renaming some of the dummy indices, and considering only the special case $\boldsymbol{r} = \boldsymbol{0}$, (5.23) becomes

$$\left\langle \frac{\partial u_i'}{\partial x_j}\frac{\partial u_i'}{\partial x_j}\right\rangle = \iiint_{-\infty}^{\infty} K^2\Phi_{ii}(\boldsymbol{K})\,\mathrm{d}\boldsymbol{K} = 2\int_0^{\infty} K^2 E(K)\,\mathrm{d}K \tag{5.24}$$

where, in the last step, we have used the definition of the energy spectrum $E(K)$ in (5.16) (note that the factor K^2 is constant when integrating over a spherical shell with radius K).

Comparison of (5.24) and (5.20) shows that the energy and dissipation spectra are related as

$$D(K) = 2\nu K^2 E(K)\quad . \tag{5.25}$$

Note especially the factor K^2, resulting in an monotonically increasing amplification of the effect of small-scale motions with high wave number. We therefore expect that the dissipation of TKE occurs at scales that are much smaller than the energy-containing scales characterized by the peak in $E(K)$. This surprising finding and its physical implications are discussed in more detail in the following.

5.2 Spectral energy transfer

5.2.1 Transport of kinetic energy

Similar to the transport equation for the Reynolds stress in (4.26), a transport equation for the two-point correlation R_{ij} can be derived. For *homogeneous* turbulence, according to (5.13) the Fourier transform of this equation yields a dynamic equation for the three-dimensional spectrum tensor $\Phi_{ij}(\boldsymbol{K}, t)$, and, after contraction and integration over a spherical shell as in (5.17), an equation for the energy spectrum $E(K, t)$. Since the derivation is rather complex (Pope, 2000), here we only discuss the properties of the final relation. Assuming in addition that turbulence is *isotropic*, the final result can be written as

$$\frac{\partial E}{\partial t} + \frac{\partial \mathcal{T}}{\partial K} = -2\nu K^2 E \,, \tag{5.26}$$

illustrating that the change of energy contained in motions with wave number K is determined by: (a) the dissipation of energy at wavenumber K (right hand side), as discussed above; (b) the divergence (in wavenumber space) of the spectral energy flux $\mathcal{T}$, which represents the exchange of energy between motions with wavenumber K, and all other wavenumbers.

According to (5.18), the integral of $E(K, t)$ over all wave numbers corresponds to the turbulent kinetic energy k. Integrating the first term in (5.26) yields

$$\int_0^\infty \frac{\partial E(K,t)}{\partial t}\,\mathrm{d}K = \frac{\mathrm{d}}{\mathrm{d}t}\int_0^\infty E(K,t)\,\mathrm{d}K = \frac{\mathrm{d}k}{\mathrm{d}t} \quad . \tag{5.27}$$

The integral of the second term (divergence of spectra energy transport) vanishes because motions with $K = 0$ (lower integration limit) correspond to the mean flow and thus contain no turbulence kinetic energy, as do motions with infitely small scales ($K = \infty$, upper integration limit). Finally, the integral of the dissipation term on the right hand side yields the turbulence dissipation rate ε as shown in the previous section.

In summary, for isotropic (and thus homogeneous) turbulence the integral of (5.26) in wavenumber space yields an equation of the form

$$\frac{\mathrm{d}k}{\mathrm{d}t} = -\varepsilon \,, \tag{5.28}$$

which, as expected, is recognized as the transport equation (4.23) for the TKE for homogeneous conditions.

5.2.2 Scales of turbulent motions

Energy spectra for turbulence have been theoretically derived by Kolmogorov (1941). He assumed that at sufficiently high Reynolds numbers the flow is locally isotropic (and thus homogenous). The term *local isotropy* refers to motions at high wavenumber (small scales) that are known to be isotropic even if the large scale turbulent motions are anisotropic. If it is further assumed that that

turbulence is in equilibrium, the spectral energy flux $\mathcal{T}$ conincides with the amount of energy ε that is dissipated at the smallest scales. For the range of motions that satisfy these conditions, all statistical parameteres should be uniquely determined by two dimensional quantities: the dissipation rate ε, and viscosity ν. These quantities have the following dimensions:

$$[\nu] = L^2T^{-1} \quad , \; [\varepsilon] = L^2T^{-3}, \tag{5.29}$$

which, for dimensional reasons, can be combined only in the following way to yield a length scale:

$$\lambda = \left(\frac{\nu^3}{\varepsilon}\right)^{1/4} \quad . \tag{5.30}$$

For motions at this scale, referred to as the *Kolmogorov scale*, the spectral energy transport towards smaller scales and the dissipation of kinetic energy into heat are of the same order of magnitude. In the following, we will also often refer to the *Komogorov wave number*, which is simply the inverse of the Kolmogorov length scale: $K_\nu = \lambda^{-1}$.

The view of turbulence at high Reynolds number is that energy is extracted from the meanflow at the low wave number range with wavenumbers of $K \approx l^{-1}$ where l is the integral (e.g., autocorrelation) scale, and K the magnitude of the wave number vector $\boldsymbol{K}$. The turbulent kinetic energy is then cascading down to higher wave numbers by vortex stretching due to the non-linear terms in the Navier-Stokes equations. When reaching the large wave numbers, where viscosity dominates, this energy is then dissipated into heat. The range of length scales much smaller than the integral length scale is called the *univeral equilibrium range*. Therefore, at sufficiently high Reynolds number, the spectrum must be of the form:

$$E = E(K, \varepsilon, \nu) \qquad K \gg l^{-1} \quad . \tag{5.31}$$

Inside the equlibrium range, there is a subrange of motions that are much larger than the Kolmogorov scale ($K \ll K_\nu$), and thus not directly affected by viscosity. This region of the energy spectrum is usually referred to as the *inertial subrange*, described by

$$E = E(K, \varepsilon) \qquad K_\nu \gg K \gg l^{-1} \, . \tag{5.32}$$

These relations form the main content of the famous *first and second similary hypotheses* of Kolmogorov (1941). In addition to these two hypotheses, Kolmogorov (1941) also formulated his *hypothesis of local isotropy*, which states that motions in the universal equilibrium range are statistically isotropic. This important result will be frequently used in the following sections.

Kolmogorov (1941) used dimensional analysis to theoretically derive the shape of the spectrum in the inertial subrange. The involved quantities have the following units:

$$\begin{aligned} [E] &= L^3T^{-2} \\ [\varepsilon] &= L^2T^{-3} \\ [K] &= L^{-1} \end{aligned} \tag{5.33}$$

which can be combined only in the following form to yield a dimensionally correct functional dependency for the inertial subrange:

$$E(K) = K_o \varepsilon^{2/3} K^{-5/3} \qquad K_\nu \gg K \gg l^{-1} \tag{5.34}$$

with the Kolmogorov constant K_o ranging between 1.4 and 1.8, depending slightly on the Reynolds number (the value of K_o cannot be found from dimensional analysis along; it has to be determined from experiments). Equation (5.34) is called *Kolmogorov's $K^{-5/3}$ law* for the inertial subrange of turbulence.

For the description of the complete univeral equilibrium range, which includes small-scale motions that are likely to feel the effect of viscosity, the fluid viscosity ν has to be taken into account as well. It is easy to show from dimensional analysis that this requires an additional depency on the Kolmogorov wave number:

$$E(K) = K_o \varepsilon^{2/3} K^{-5/3} f(K/K_\nu) \qquad K \gg l^{-1} \tag{5.35}$$

where $f(K/K_\nu)$ is a non-dimensional function that has to be determined from experiments or theoretical models that are beyond the scope of this lecture. Several formulations have been suggested for f (Pope, 2000), among them the Kovasznay spectrum,

$$f(K\lambda) = \left(1 - 0.5 K_o (K/K_\nu)^{4/3}\right)^2 \ , \tag{5.36}$$

the Heisenberg spectrum,

$$f(K\lambda) = \left(1 + (1.5K_o)^2 (K/K_\nu)^4\right)^{-4/3} \ , \tag{5.37}$$

and the Pao spectrum,

$$f(K\lambda) = \exp\left(-1.5 K_o (K/K_\nu)^{4/3}\right) \quad . \tag{5.38}$$

The universal character of the energy spectrum in the universal equlibrium range becomes especially clear by re-writing (5.35) in non-dimensional form:

$$\frac{E(K)}{(\epsilon\nu^5)^{1/4}} = K_o \left(K/K_\nu\right)^{-5/3} f\left(K/K_\nu\right) \qquad K \gg l^{-1} \ , \tag{5.39}$$

which only depends on the non-dimensinal wave number K/K_ν. Similarly, the dissipation spectrum $D(K) = 2\nu K^2 E(K)$ defined in (5.25) can be non-dimensionalized for the universal equilibrium range, and written as follows:

$$\frac{D(K)}{(\epsilon\nu)^{3/4}} = 2K_o \left(K/K_\nu\right)^{1/3} f\left(K/K_\nu\right) \qquad K \gg l^{-1} \quad . \tag{5.40}$$

The spectral shapes in (5.39) and (5.40) apply to *any* turbulent flow at sufficiently high Reynolds number, ranging from small-scale turbulent engineering flows to large-scale geophysical flows in the atmosphere, oceans, and in gaseous

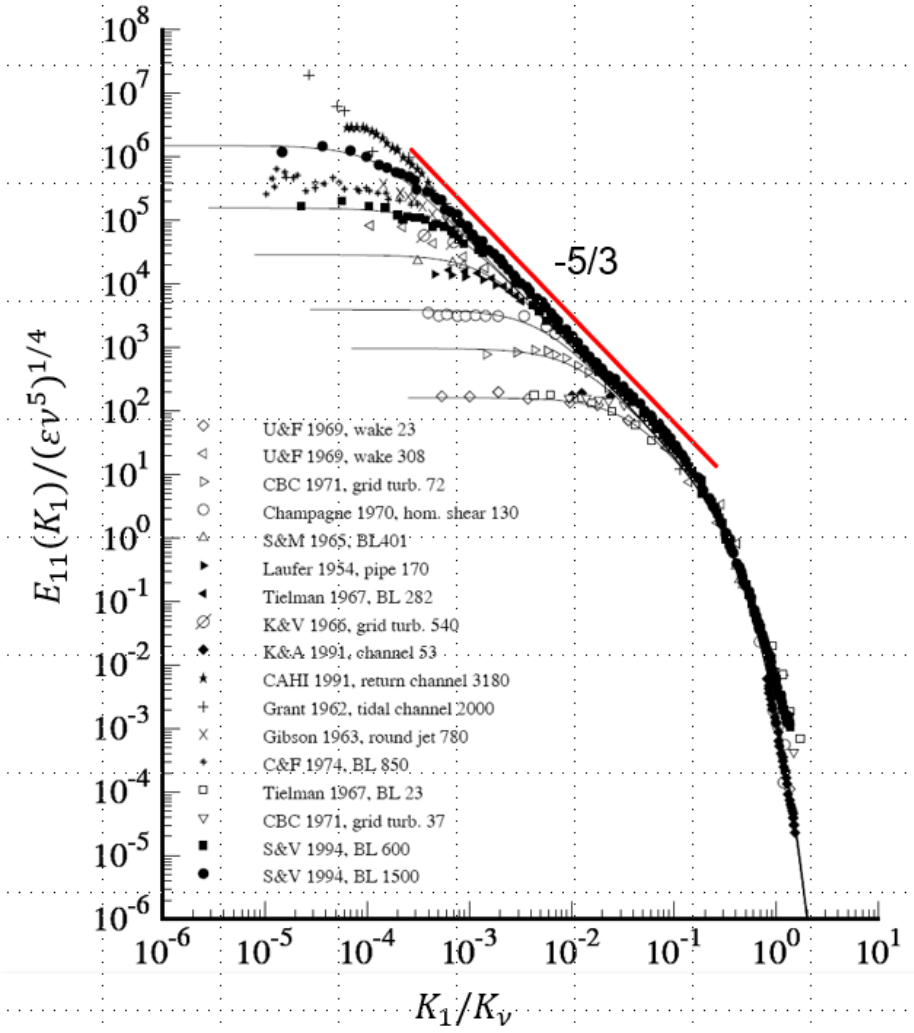

Figure 5.3: Non-dimensional spectra from various data sources. Figure taken from Pope (2000).

stars like our sun. Its importance can hardly be overestimted. The power of (5.39) becomes particularly clear from Figure 5.3, showing that the high-wave number part of energy spectra from various contexts and scales (ranging from laboratory data to energetic tidal currents in the ocean) collapse onto a single curve if non-dimsionalized according to (5.39).

The different suggestions for the universal spectra in (5.36) - (5.38) are shown in Figure 5.4. For non-dimensional wave numbers smaller than $K/K_\nu \approx 0.1$, all energy spectra are seen to converge towards the $-5/3$ slope of the inertial subrange. For higher wave numbers, the spectra show a rapid roll-off with only relatively small differences observed between the different models. Also the dissipation spectra shown in Figure 5.4b converge towards the predicted inertial-subrange slope (1/3 in this case). For higher wave numbers, however, they continue to increase up to the dissipation peak (black markers) before they decay again. The dissipation peaks for the different models are reached for non-dimensional wave numbers in the range $K/K_\nu \approx 0.2 - 0.3$. Recalling that motions of wave number K have a length scale of $L = 2\pi/K$, this suggests that the dissipation peak is reached for $L \approx 20 - 30\lambda$, depending on the model. Similarly, energy dissipation becomes negligible for $K/K_\nu \approx 1$ (Figure 5.4b), corresponding to motions larger than $L \approx 2\pi\lambda$. For orientation, turbulence in the ocean ($\nu = 10^{-6}$ m^2 s^{-1}) ranges from values around $\varepsilon = 10^{-10}$ W kg^{-1} in the quiescent deep layers up to $\varepsilon = 10^{-3}$ W kg^{-1} in the energetic near-surface region under storm conditions. These values correspond to a range of λ between 1 cm (deep ocean) and a few tens of a millimeter. This illustrates the extremely small scales of turbulence that poses a serious challenge to both numerical modeling and observations.

5.3 One-dimensional energy spectra

It should be recalled that the energy spectrum $E(K, t)$ involves the magnitude of the wavenumber vector $\boldsymbol{K}$, which is notoriously difficult to observe due to its three-dimensional nature. Typical oceanic instrumentation can only provide vertical or horizontal profiles of different velocity components, from which K cannot be derived without further assumptions. Nevertheless, relationships between the full and the one-dimensional energy spectra can be derived for the idealised case of isotropic turbulence. In isotropic turbulence, no preferred direction exists, such that the off-diagonal terms of the Reynolds stress tensor vanish: $\left\langle u_i' u_j' \right\rangle = 2/3k\delta_{ij}$. In this case, turbulence supports neither momentum flux nor shear production, the latter implying that unstratified isotropic turbulence always decays in time. The difference between isotropic and anisotropic turbulence is illustrated in Figure **??**.

5.3.1 General definitions

The argumentation in this section follows mostly the excellent text book by Pope (2000). For simplicity, we identify the direction in which one-dimensional

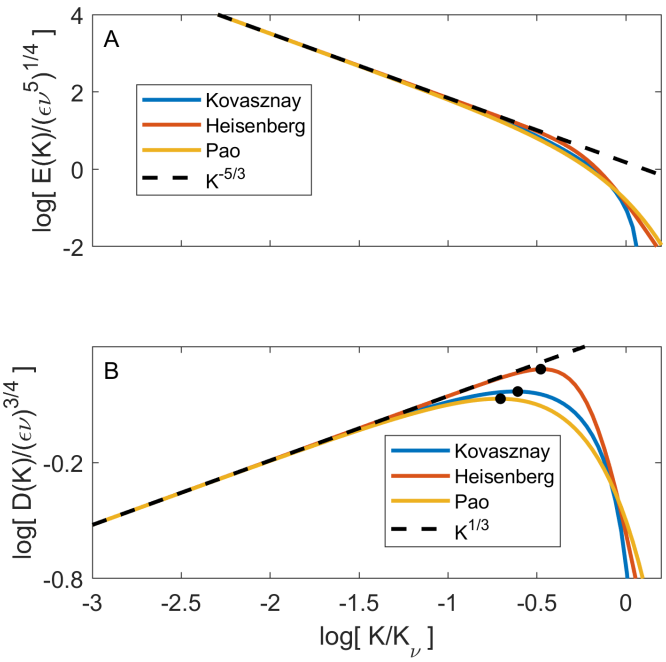

Figure 5.4: Non-dimensional spectral shapes for the universal equilibrium range for (a) the energy spectrum $E(K)$ and (b) dissipation spectrum $D(K)$ using $K_o = 1.5$ for the Kolmogorov constant. Black markers in (b) indicate the dissipation peak.

measurements are taken with the x_1 axis. We distinguish between fluctuations of the velocity component parallel to this axis (longitudinal spectra), and those orthogonal to this axis (transverse spectra). One-dimensional spectra are then defined as:

$$E_{ij}(K_1) = \frac{1}{\pi}\int_{-\infty}^{\infty} R_{ij}(\boldsymbol{e}_1 r_1) e^{-iK_1 r_1} \mathrm{d}r_1 \ , \tag{5.41}$$

from which we infer the longitudinal spectrum,

$$E_{11}(K_1) = \frac{1}{\pi}\int_{-\infty}^{\infty} R_{11}(\boldsymbol{e}_1 r_1) e^{-iK_1 r_1} \mathrm{d}r_1 = \frac{2}{\pi}\int_{0}^{\infty} R_{11}(\boldsymbol{e}_1 r_1)\cos(K_1 r_1)\mathrm{d}r_1 \ , \tag{5.42}$$

and the transverse spectrum:

$$E_{22}(K_1) = \frac{1}{\pi}\int_{-\infty}^{\infty} R_{22}(\boldsymbol{e}_1 r_1) e^{-iK_1 r_1} \mathrm{d}r_1 = \frac{2}{\pi}\int_{0}^{\infty} R_{22}(\boldsymbol{e}_1 r_1)\cos(K_1 r_1)\mathrm{d}r_1 \quad . \tag{5.43}$$

The cosine expansions have been derived from the fact that both R_{11} and R_{22} are real and symmetric in r_1. The inverse transform for the longitudinal correlation then follows from

$$R_{11}(\boldsymbol{e}_1 r_1) = \int_{0}^{\infty} E_{11}(K_1)\cos(K_1 r_1)\mathrm{d}K_1 \ , \tag{5.44}$$

and an equivalent expression for the transverse correlation, $R_{22}(\boldsymbol{e}_1 r_1)$. Note that

$$R_{11}(\boldsymbol{0}) = \langle {u'}_1^2 \rangle = \int_{0}^{\infty} E_{11}(K_1)\mathrm{d}K_1 \ , \tag{5.45}$$

and

$$R_{22}(\boldsymbol{0}) = \langle {u'}_2^2 \rangle = \int_{0}^{\infty} E_{22}(K_1)\mathrm{d}K_1 \ , \tag{5.46}$$

denote the variance (or twice the kinetic energy) in the longitudinal and transverse velocity fluctuations. Both coincide only in the case of isotropic turbulence.

As discussed in more detail in Section A.4, for the special case of isotropic turbulence, it can be shown that the most general functional form for the relation $R_{ij}(\boldsymbol{r})$ is represented by a linear combination of the two second-order tensors δ_{ij} and $r_i r_j$. The linear factors combining these two tensors can only depend on $r = |\boldsymbol{r}|$, which is the only invariant of $\boldsymbol{r}$ (i.e. it does not change when $\boldsymbol{r}$ is rotated). It is customary to formulate this functional relationship mathematically in the following form:

$$R_{ij}(\boldsymbol{r}) = \langle u'^2 \rangle \left(g(r)\delta_{ij} + (f(r) - g(r))\,\frac{r_i r_j}{r^2} \right) \ , \tag{5.47}$$

where $\langle u'^2 \rangle$ equals $\langle {u'}_1^2 \rangle = \langle {u'}_2^2 \rangle = \langle {u'}_3^2 \rangle$.

Arbitrarily choosing $\boldsymbol{r} = \boldsymbol{e}_1 r_1$, we find

$$\begin{aligned} f(r) &= \frac{R_{11}(\boldsymbol{e}_1 r_1)}{\langle u'^2 \rangle} \ , \\ g(r) &= \frac{R_{22}(\boldsymbol{e}_1 r_1)}{\langle u'^2 \rangle} \ , \end{aligned} \tag{5.48}$$

which identifies f and g as the longitudinal and transverse correlation functions, respectively. Isotropy further implies the following relationships:

$$\begin{aligned} R_{22}(\boldsymbol{e}_1 r_1) &= R_{33}(\boldsymbol{e}_1 r_1) \ , \\ R_{ij}(\boldsymbol{e}_1 r_1) &= 0, \text{ for } i \neq j \quad . \end{aligned} \tag{5.49}$$

Using the incompressibility condition $\partial R_{ij}/\partial r_j = 0$, we can derive the following relation from (5.47):

$$g(r) = f(r) + \frac{1}{2} r \frac{\mathrm{d}f}{\mathrm{d}r} \tag{5.50}$$

where we have used the auxiliary relations

$$\frac{\partial r}{\partial r_i} = \frac{r_i}{r} \tag{5.51}$$

and

$$\frac{\partial}{\partial r_j}\left(\frac{r_i r_j}{r^2}\right) = \frac{2 r_i}{r^2}. \tag{5.52}$$

We conclude that for homogeneous, isotropic turbulence all information about the one-dimensional correlation tensor is contained in a single scalar function: the longitudinal correlation function $f(r)$.

With (5.48) the spectra $E_{11}(K_1)$ and $E_{22}(K_1)$ may be expressed:

$$E_{11}(K_1) = \frac{2}{\pi} \langle u'^2 \rangle \int_0^\infty f(r) \cos(K_1 r) \, \mathrm{d}r \ , \tag{5.53}$$

and

$$E_{22}(K_1) = \frac{2}{\pi} \langle u'^2 \rangle \int_0^\infty g(r) \cos(K_1 r) \, \mathrm{d}r \quad . \tag{5.54}$$

Similar to the temporal integral scale $\mathcal{T}$ defined in (5.5), the longitudinal and transverse integral length scales l_{11} and l_{22}, respectively, are defined as the integral of the corresponding correlation functions:

$$l_{11} = \int_0^\infty f(r) \, \mathrm{d}r \ , \tag{5.55}$$

and

$$l_{22} = \int_0^\infty g(r) \, \mathrm{d}r \quad . \tag{5.56}$$

5.3.2 Conversion relations

The question now is how the one dimensional spectra defined above are related to the three-dimensional spectrum $E(K)$ defined in (5.16). To this end, we start from the general definition of the three-dimensional spectrum tensor in (5.14), considering only the special case $i = j = 1$ and $\boldsymbol{r} = \boldsymbol{e}_1 r_1$:

$$\begin{aligned} R_{11}(\boldsymbol{e}_1 r_1) &= \iiint_{-\infty}^{\infty} \Phi_{11}(\boldsymbol{K}) e^{iK_1 r_1} \,\mathrm{d}K_1 \,\mathrm{d}K_2 \,\mathrm{d}K_3 \\ &= \int_{-\infty}^{\infty} \left(\iint_{-\infty}^{\infty} \Phi_\theta(\boldsymbol{K}) \,\mathrm{d}K_2 \,\mathrm{d}K_3 \right) e^{iK_1 r_1} \,\mathrm{d}K_1 \\ &= \int_{-\infty}^{\infty} \frac{1}{2} E_{11}(K_1) e^{iK_1 r_1} \mathrm{d}K_1 \\ &= \int_0^{\infty} E_{11} dd(K_1) \cos(K_1 r_1) \mathrm{d}K_1 \ , \end{aligned} \tag{5.57}$$

from which by comparision with (5.44) we conclude that

$$E_{11}(K_1) = 2 \iint_{-\infty}^{\infty} \Phi_{11}(\boldsymbol{K}) \,\mathrm{d}K_2 \,\mathrm{d}K_3 \quad . \tag{5.58}$$

The relation for the transverse one-dimensional spectrum follows from an analogous relation:

$$E_{22}(K_1) = 2 \iint_{-\infty}^{\infty} \Phi_{22}(\boldsymbol{K}) \,\mathrm{d}K_2 \,\mathrm{d}K_3. \tag{5.59}$$

To evalute the integrals on the right hand sides of (5.58) and (5.59), it is helpful to consider the special shape of the velocity spectrum tensor $\Phi_{ij}(\boldsymbol{K})$ for the case of isotropic turbulence. Analogously to the isotropic tensor function in (5.47) for the correlation tensor, we know that the isotropic relation for the spectrum tensor must be of the following form (see Section A.4):

$$\Phi_{ij}(\boldsymbol{K}, t) = A(K, t)\delta_{ij} + B(K, t) K_i K_j \ , \tag{5.60}$$

Using the incompressibility condition (see assignments),

$$K_j \Phi_{ij} = 0 \ , \tag{5.61}$$

we obtain a relation

$$B(K, t) = -\frac{A(K, t)}{K^2} \tag{5.62}$$

for the coefficients appearing in (5.60). Without loss of generality, (5.60) may therefore be re-written in the following form

$$\Phi_{ij}(\boldsymbol{K}, t) = A(K, t) \left(\delta_{ij} - \frac{K_i K_j}{K^2} \right). \quad . \tag{5.63}$$

We now set $i = j$ in (5.63), and integrate over the surface of a sphere with radius K according to (5.17):

$$\begin{aligned} E(K) &= \oint \frac{1}{2}\Phi_{ii}(\boldsymbol{K})\mathrm{d}\mathcal{S}(K) \\ &= \oint \frac{1}{2}A(K)\left(\delta_{ii} - \frac{K_i K_i}{K^2}\right)\mathrm{d}\mathcal{S}(K) \\ &= \oint \frac{1}{2}A(K)\,(3-1)\,\mathrm{d}\mathcal{S}(K) \\ &= A(K)\oint \mathrm{d}\mathcal{S}(K) \\ &= A(K)4\pi K^2 \quad . \end{aligned} \tag{5.64}$$

Using this result, we find

$$A(K) = \frac{E(K)}{4\pi K^2}\,, \tag{5.65}$$

allowing us the express the spectrum tensor in terms of the energy spectrum according to

$$\Phi_{ij}(\boldsymbol{K}) = \frac{E(K)}{4\pi K^2}\left(\delta_{ij} - \frac{K_i K_j}{K^2}\right) \quad . \tag{5.66}$$

Now we come back to our original goal of evaluating the right hand side of (5.58), which can be re-written as

$$E_{11}(K_1) = \iint_{-\infty}^{\infty} \frac{E(K)}{2\pi K^2}\left(1 - \frac{K_1^2}{K^2}\right)\mathrm{d}K_2\,\mathrm{d}K_3. \quad . \tag{5.67}$$

The integration over the K_2-K_3 plane in (5.67) is easiest performed by introducing the polar (radial) coordinate

$$K_r = \sqrt{K_2^2 + K_3^2} \quad \Rightarrow \quad K_r^2 = K^2 - K_1^2 \tag{5.68}$$

where it should be recalled that the wave number is defined as $K = \sqrt{K_1^2 + K_2^2 + K_3^2}$. Since the integrand is radially symmetric, (5.67) can be expressed as

$$E_{11}(K_1) = \int_0^{\infty} \frac{E(K)}{2\pi K^2}\left(1 - \frac{K_1^2}{K^2}\right)2\pi K_r \mathrm{d}K_r. \tag{5.69}$$

With (5.68), we see that $K_r \mathrm{d}K_r = K\mathrm{d}K$, and $K(K_r = 0) = K_1$ such that (5.69) can be reformulated into

$$E_{11}(K_1) = \int_{K_1}^{\infty} \frac{E(K)}{K}\left(1 - \frac{K_1^2}{K^2}\right)\mathrm{d}K \quad . \tag{5.70}$$

The corresponding relation for the transverse spectrum is obtained in a similar way (not shown), yielding:

$$E_{22}(K_1) = \frac{1}{2}\int_{K_1}^{\infty} \frac{E(K)}{K}\left(1+\frac{K_1^2}{K^2}\right)\,\mathrm{d}K \quad . \tag{5.71}$$

The use of (5.70) and (5.71) allows the conversion of arbitrary model spectra for $E(K)$ into the corresponding one-dimensional spectra, obtained e.g. from measurements. As an example, let's assume that the model spectra obey a certain power-law form as in Section 5.2.2:

$$E(K) = CK^{-p} \quad . \tag{5.72}$$

Inserting this relation into (5.70) and (5.71), it is easy to show that $E_{11} = C_{11}K^{-p}$ and $E_{22} = C_{22}K^{-p}$. The one-dimensional spectra thus follow the same power-law behavior, however, with different constants $p(p+2)C_{11} = 2C$ and $p(p+2)C_{22} = (p+1)C$. For the Kolmogorov spectrum (5.34), valid in the inertial subrange, we find

$$E_{11}(K_1) = \frac{18}{55}K_0\varepsilon^{2/3}K_1^{-5/3}\,, \tag{5.73}$$

and

$$E_{22}(K_1) = \frac{24}{55}K_0\varepsilon^{2/3}K_1^{-5/3} \quad . \tag{5.74}$$

These relation are for example useful to infer the dissipation rate from the spectral slopes of measured one-dimensional spectra.

Chapter 6

Statistical turbulence models

The closure problem of turbulence has already been introduced in section 4.5. Turbulence modelling is a way to close the mathematical equations by means of introducing empirical parameterisations. Depending which statistical moments are used to close the system, we talk about first-moment, second-moment or even higher-moment turbulence closures models. Using this definition, models solving dynamic transport equations for the first statistical moments (the means) are called first-moment closures. In second-moment closure models, dynamic equations for the second statistical moments are solved, e.g. for the the TKE, k, or for the Reynolds-stresses $\left\langle u_i' u_j' \right\rangle$.

6.1 Eddy viscosity principle

One of the basic principles of turbulence modelling is the so-called eddy viscosity assumption first formulated by Boussinesq. This is easiest understood by considering a simple one-dimensional flow, $\bar{u} = \bar{u}(z)$, that is assumed to homogenous in the x- and y-directions. The total stress in the Reynolds-averaged Navier-Stokes equations (4.15) may be formulated as:

$$\tau = \tau_m + \tau_t = \rho_0 \left(\nu \partial_z \bar{u} - \langle u' w' \rangle \right). \tag{6.1}$$

Now let's write the Reynolds stress according to

$$- \langle u' w' \rangle = \nu_t \partial_z \bar{u}, \tag{6.2}$$

with the so-called eddy viscosity ν_t, which is still completely general because nothing has been said about the dependency (or even the sign) of ν_t. Combining (6.1) and (6.2), we finally obtain:

$$\tau = \tau_m + \tau_t = \rho_0 \left(\nu + \nu_t \right) \partial_z \bar{u}. \tag{6.3}$$

Unlike the molecular viscosity, which varies only slightly with temperature and is thus usually considered as a material constant, the eddy viscosity is highly variable in time and space. For high-Reynolds number flows, it is typicall many orders of magnitude larger than the molecular viscosity. A generalisation of (6.2) to non-idealised three-dimensional flows would be of the following form

$$-\langle u_i' u_j' \rangle = \nu_t \bar{S}_{ij} - \frac{2}{3} k \delta_{ij} . \,, \tag{6.4}$$

where $\bar{\boldsymbol{S}}$ is the symmetric part of the mean velocity gradient defined in (2.4). The last term in (6.4) is required to insure consistency with the definition of the TKE for the case $i = j$ (contraction). It is important to note that, in contrast to the one-dimensional version in (6.2), the three-dimensional formulation in (6.4) does contain a modeling assumption: it assumes that the Reynolds stress tensor and the rate of strain tensor are aligned. This is often the case, but not always.

Similarly, the eddy diffusivity for a scalar quantity c is defined analogously:

$$-\langle u_i' c' \rangle = \nu_t^c \partial_i \bar{c} \,, \tag{6.5}$$

where c may be, e.g., potential temperature θ or salinity S.

6.2 Mixing length approach

Prandtl and Kolmogorov suggested to parameterise the eddy viscosity and diffusivity in a way motivated by molecular diffusion: as the product of a characteristic length l, and a characteristic velocity, q:

$$\nu_t = l \cdot q \quad . \tag{6.6}$$

For a gas, statistical mechanics predicts that q is proportional to the speed of sound, and l to the mean free path of the gas molecules. In turbulence, however, such a generally valid relation cannot be found. Nevertheless, in a number of simple turbulent flows, Prandtl's *mixing length approach*, was found to lead to reasonable predictions. There are several ways of motivating the closure assumptions involved but the most straighforward interpretation is the one considering time scales. To this end, we start from the simple one-dimensional flow considered in the context of (6.1), noting that the only time scale imposed by the mean flow is $(\partial \bar{u}/\partial z)^{-1}$. The only turbulence time scale that can be constructed from q and l is l/q, which can be thought of as a typical eddy turnover time scale. The mixing length model assumed that both time scales are proportional:

$$\frac{q}{l} \propto |\partial_z \bar{u}| \tag{6.7}$$

such that

$$\nu_t = l^2 \left| \frac{\partial \bar{u}}{\partial z} \right| \quad . \tag{6.8}$$

This relation predicts strictly positive diffusivities proportional to the mean velocity gradient. The relation can be generalized to three-dimensions, which is, however, not discussed here. With these modeling assumptions, the Reynolds stress may be formulated as

$$\tau_t = -\rho_0 \langle u'w' \rangle = \rho_0 \nu_t \partial_z \bar{u} = \rho_0 l^2 \frac{\partial \bar{u}}{\partial z} \left| \frac{\partial \bar{u}}{\partial z} \right| , \tag{6.9}$$

illustrating that the closure problem is reduced to finding an appropritate model for the mixing length l. This is relatively simple in simple geometries such as for flows over a solid surface.

6.3 Open channel flow

Let us consider a non-rotating, unstratified, and stationary flow in a straight channel of depth H. Assuming that the flow is unidirectional and homogenous along the x-direction, the Reynolds equations (4.15) represent a balance between the (constant) pressure-gradient and frictional effects:

$$\frac{\partial}{\partial z} \left(-\nu \partial_z \bar{u} + \langle u'w' \rangle \right) = -\frac{1}{\rho_0} \frac{\partial \bar{p}}{\partial x} , \tag{6.10}$$

or, inserting (6.1), more compactly as

$$\frac{\partial \tau}{\partial z} = \frac{\partial \bar{p}}{\partial x} \quad . \tag{6.11}$$

For non-zero $\partial_x \bar{p}$ and zero surface stress ($\tau_s = 0$), (6.11) may be integrated to yield a linear variation of the total stress

$$\tau(z) = \left(1 - \frac{z}{H} \right) \tau_b , \tag{6.12}$$

where τ_b denotes the bottom stress. Note that the pressure-gradient and the bottom stress are related by

$$\tau_b = -H \frac{\partial p}{\partial x} , \tag{6.13}$$

indicating that they are no independent quantities in this particular flow. The bottom shear stress is often expressed in non-dimensional form via the drag coefficient,

$$C_d = \frac{\tau_b}{\rho_0 U^2} , \tag{6.14}$$

where U is some suitably defined bulk velocity, e.g. the vertically averaged velocity.

6.3.1 Non-dimensional description

From the geometry of the problem outlined above it is clear that $\bar{u}$ can only be a function of density ρ_0, bottom stress τ_b, viscosity ν, channel depth H, and the distance from the bed, z:

$$\bar{u} = f(\rho_0, \tau_b, \nu, H, z) \quad . \tag{6.15}$$

This functional dependency assumes that the wall is *hydrodynamically smooth*, i.e. that no additional parameters (roughness length) describing the properties of the wall appear in (6.15).

We now attempt to reduce this dependency on 5 dimensional parameters by combining them into non-dimensional products. To this end, we first note that ρ_0 and τ_b are the only parameters containing the dimension of mass, and thus have to appear in combined form, e.g. as in

$$u_* = \sqrt{\frac{\tau_b}{\rho_0}} \tag{6.16}$$

which defines the *friction velocity*. The viscous length-scale ν/u_* based on this parameter can be used to non-dimensionalize the distance from the wall

$$z^+ = \frac{z u_*}{\nu} \, , \tag{6.17}$$

such that the non-dimensional version of (6.15) can be written as

$$\frac{\bar{u}}{u_*} = F(z^+, z/H) \quad . \tag{6.18}$$

While this non-dimensional form of the velocity is completely general, it turns out to be more convenient considering the vertical shear, $\mathrm{d}\bar{u}/\mathrm{d}z$, instead of the velocity itself. Using similar dimensional arguments as above, this yields to a non-dimensional expression of the form:

$$\frac{\mathrm{d}\bar{u}}{\mathrm{d}z} = \frac{u_*}{z} \Phi(z^+, z/H) \quad . \tag{6.19}$$

6.3.2 Law of the wall

Very close to the wall ($z/H \ll 1$), at high Reynolds number, there is an *inner layer* in which the dependency on z/H in (6.19) becomes vanishingly small. As a working definition, this inner layer is usually taken as the region with $z < 0.1H$. The general expression (6.19) then reduces to

$$\frac{\mathrm{d}\bar{u}}{\mathrm{d}z} = \frac{u_*}{z} \Phi_I(z^+) \, , \qquad \text{for } z/H \ll 1 \, , \tag{6.20}$$

or, introducing the parameter $u^+ = \bar{u}/u_*$:

$$\frac{\mathrm{d}u^+}{\mathrm{d}z^+} = \frac{1}{z^+} \Phi_I(z^+) \quad . \tag{6.21}$$

This is the differential form of the *law of the wall*, forming one of the corner stones for the description of wall-bounded shear-flows flows.

The viscous sublayer

Directly at the wall, we have $u^+ = 0$ from the no-slip boundary condition, and $\mathrm{d}u^+/\mathrm{d}z^+ = 1$ from the viscous stress law (the turbulent stresses vanish very close to the wall). We therefore expect that, to first order, $\Phi_I(z^+)$ can be expressed by the first term of a Taylor series expansion as $\Phi_I = z^+$. Integration of (6.21) then yields

$$u^+ = z^+ \,, \tag{6.22}$$

or, in dimensional form,

$$\bar{u} = \frac{\tau_b}{\rho_0 \nu}\, z \quad . \tag{6.23}$$

The above relations predict a linear increase of the velocity profile in the *viscous sublayer*. Laboratory data and numerical simulations have demonstrated that this particular form of the law of the wall is a very good approximatation for $z^+ < 5$, with errors increasing above 25 percent for $z^+ > 12$.

The log layer

Close to the wall, the velocity and length scales of turbulent eddies scale with u_* and z, because there are no other relevant velocity and length scales. This implies that the non-dimensional parameter z^+ defined in (6.17) can be interpreted as the Reynolds number relevant for eddies at distance z from the wall. As with any other turbulent flow, for increasing Reynolds the relative importance of viscous effects decreases such that for z^+ exceeding a certain threshold viscous effects may be entirely disregarded. Mathematically, the dependency of Φ_I on z^+ (depending on viscosity) has to vanish, and Φ_I becomes a constant:

$$\Phi_I = \frac{1}{\kappa} \,, \qquad \text{for } z^+ \gg 1 \text{ and } z/H \ll 1 \quad . \tag{6.24}$$

where κ is the so-scalled von Kármán constant. Laboratory data indicate that for $z^+ > 50$, the viscous stress becomes insignificant compared to the turbulent stress. Under these conditions, (6.21) becomes

$$\frac{\mathrm{d}u^+}{\mathrm{d}z^+} = \frac{1}{\kappa z^+} \,, \tag{6.25}$$

which integrates to

$$u^+ = \frac{1}{\kappa} \ln z^+ + B \,, \tag{6.26}$$

where B is an integration constant. The model constants exhibit some variability but generally they are within a few percent of $\kappa = 0.41$ and $B = 5.2$. The logarithmic behavior in (6.26) shows excellent agreement with available data already for $z^+ > 30$. This layer is often called the *log layer*, extending until $z \approx 0.3H$. The region between $z^+ = 5$ and $z^+ = 30$ is called the *buffer layer*, for which no analytical solution can be found.

6.3.3 Model description

Since the log law is a crucial component of the flow near a rigid wall, we expect a turbulence model to reproduce this behavior. With this in mind, in the following we investigate the performance of the simple mixing length model (6.9) for wall bounded shear flows. In a first step, we consider a flow without pressure-gradients that is exclusively driven by a stress at the surface $z = H$ pointing into the x-direction. Let's assume, as before, that the flow is stationary, non-rotating, unstratified, and unidirectional in the horizontal x-direction. This geometry is often referred to as a *Couette flow*. Assuming that we are outside the viscous sublayers at the upper and lower boundaries, it is easy to show that the Reynolds stress is constant:

$$\frac{\tau}{\rho_0} = u_*^2 = -\langle u'w' \rangle = \text{ const.} \tag{6.27}$$

Since the shear is positive for the given geometry, inserting the mixing length model (6.9) into (6.27) yields

$$l \frac{\mathrm{d}\bar{u}}{\mathrm{d}z} = u_* \, , \tag{6.28}$$

which cannot be integrated without an additional closure assumption for the turbulent length scale l. The only available length scale in this problem, however, is the distance from the wall, indicating that the turbulent eddies scale with the wall distance. This leads to

$$l = \kappa z \, , \tag{6.29}$$

where κ is a model constant. Using this result, integration of (6.28) finally leads to

$$\frac{\bar{u}}{u_*} = \frac{1}{\kappa} \ln z^+ + B \, , \tag{6.30}$$

where B is a constant. Comparison with (6.26) illustrates that the mixing length model predicts the log law in perfect agreement with the functional form derived from purely dimensional arguments.

In modeling studies, (6.30) is often reformulated in slightly different form. To this end, we first note that the location of $\bar{u} = 0$ is located at $z_0^+ = \exp(-\kappa B) \approx 0.13$, clearly outside the validity of the logarithmic law of the wall. For this reason, the location $z^+ = z_0^+$ is often referred to as the "virtual origin" of the log law. In dimensional notation, this can be expressed as

$$z_0 = \frac{z_0^+ \nu}{u_*} \approx 0.13 \frac{\nu}{u_*} . \, , \tag{6.31}$$

which is combined with (6.30) to yield the following alternative form of the log law:

$$\frac{\bar{u}(z)}{u_*} = \frac{1}{\kappa} \ln \left(\frac{z^+}{z_0^+} \right) = \frac{1}{\kappa} \ln \left(\frac{z}{z_0} \right) . \tag{6.32}$$

For hydrodynamically rough beds with the length of roughness elements K_0, the viscous sublayer is completely submerged in the roughness elements and (6.32) is valid outside the roughness elements with $z_0 \approx K_0/30$.

6.4 One-equation models

One of the corner stones of turbulence modeling is the transport equation (4.23) for the turbulent kinetic energy, k. We will base our introduction of modeling concepts on this equation as well. For simplicity, as above, we consider only boundary-layer flows in which all horizontal gradients can be ignored. If it is additionally assume that the flow is aligned with the x-direction (along the boundary), the TKE budget in (4.23) can be written as

$$\frac{\partial k}{\partial t} + \frac{\partial \mathcal{T}_k}{\partial z} = P + G - \varepsilon \ , \tag{6.33}$$

where shear production P and shear S are defined as

$$P = -\langle u'w' \rangle S \ , \qquad S = \frac{\partial \bar{u}}{\partial z} \ , \tag{6.34}$$

and the buoyancy production as

$$G = \langle w'b' \rangle = -\frac{g}{\rho_0} \langle w'\rho' \rangle \quad . \tag{6.35}$$

The term $\mathcal{T}_k$ is sum of all transport terms.

6.4.1 Modeling assumptions

Several "closure assumptions" are required to close the TKE budget (6.33). One important assumption typically made in one-equation models of this type is that the turbulent fluxes can be expressed with "down-gradient" formulations, introducing turbulent diffusivities as discussed above in the context of (6.2). This allows us to write the shear and buyancy production terms in (6.34) and (6.35), respectively, in the form

$$P = \nu_t S^2 \ , \qquad G = -\nu_t^b N^2 \ , \tag{6.36}$$

where $N^2 = \partial \bar{b}/\partial z$ is the buoyancy gradient (or the square of the buoyancy frequency N), defined in terms of the mean buoyancy $\bar{b} = -g(\bar{\rho} - \rho_0)/\rho_0$.

Following (6.6), the vertical diffusivity of momentum is modeled as the product of a turbulent length and velocity scales, the latter taken proportional to the square root of k:

$$\nu_t = c_l l k^{1/2} \ , \tag{6.37}$$

where c_l is a model constant. The ratio of the diffusivities for momentum and density (buoyancy) is the Prandtl number defined as:

$$P_r^t = \frac{\nu_t}{\nu_t^b} \ , \tag{6.38}$$

which is of the order of unity for weakly stratified flows but may increase strongly with increasing stratification. Here, for simplicity, we assume that P_r^t is constant. Finally, a diffusion model is used to describe the vertical transport of TKE:

$$\mathcal{T}_K = -\frac{\nu_t}{\sigma_k} \frac{\partial k}{\partial z} \ , \tag{6.39}$$

with the constant *Schmidt number* σ_k.

Next, we attempt to model the energy dissipation, occuring at the smallest scales with the help of known large-scale parameters. The key to this is the energy cascade that we have studied in the previous chapter. Integrating the Kolmogorov spectrum (**??**) from any wave number K_I (located inside the inertial subrange) to infinity, it is easy to show $\varepsilon \propto k_I^{3/2}/l_I$, where $l_I = 2\pi/K_I$ is the size of eddies at wave number K_I, and k_I is the energy contained in motions with $K \geq K_I$. Although (**??**) is not valid for motions outside the inertial subrange, it can be shown that the relation found above also holds for the energy containing scales that are usually much larger than the scales of the inertial subrange. The result is a widely applicable relation between the small scale dissipation rate, and the large-scale parameters l and k:

$$\varepsilon = c_\mu \frac{k^{3/2}}{l} \ , \tag{6.40}$$

where c_μ is model constant. Alternatively, (6.40) can be derived from the assumption that the time scale k/ε for energy dissipation is proportional to the eddy turnover time scale, $l/k^{1/2}$. This argument hence assumes that eddies loose an appreciable fraction of their kinetic energy during one turnover, and leads directly to (6.40).

Implementing all modeling assumptions into the TKE budget in (6.33), we find an equation of the form:

$$\frac{\partial k}{\partial t} - \frac{\partial}{\partial z}\left(\frac{\nu_t}{\sigma_t}\frac{\partial k}{\partial z}\right) = \nu_t\left(S^2 - \frac{1}{P_r^t}N^2\right) - c_\mu\frac{k^{3/2}}{l} \ , \tag{6.41}$$

where ν_t is a function of k and l according to (6.37). In conclusion, the problem can be closed if the a model for the turbulent length scale is available.

6.4.2 Describing the mixing length scale

We have seen already in the context of (6.29) that the turbulent length scale close to the boundary ("wall") scales with the distance d to the boundary: $l = \kappa d$. We expect that any model for l converges to this linear dependency in the vicinity of the upper and lower boundaries. Further, we recall that the mixing length model was derived from (6.7), stating that the eddy turnover time scale $l/k^{1/2}$ is proportional to the time scale $(\partial\bar{u}/\partial z)^{-1}$ set by the shear. In the previous sections, we have seen that this assumption is also consistent with the law of the wall. In stratified flows, however, a second time scale is introduced by the buoyancy frequency N. Data and theoretical investigations have shown that the eddy turnover time scale in stratified shear flows is limited by N^{-1} such that

$$\frac{l}{k^{1/2}} \leq cN^{-1} \ , \tag{6.42}$$

where c is a constant. The marginal case usually sets the length scale under strong stratification. It is interesting to note that combining (6.40) and (6.42),

it is easy to show that the length scale l has an upper bound that is proportional to the so-called Ozmidov scale

$$L_o = \left(\frac{\varepsilon}{N^3}\right)^{\frac{1}{2}} \quad , \tag{6.43}$$

which is of central importance in studying stratified turbulence.

A simple algebraic approximation for the mixing length l in a stratied shear flow through a channel of depth H would e.g. be of the following form:

$$l = \left(\frac{1}{\kappa z\left(1-\frac{z}{H}\right)^{1/2}} + \frac{1}{c\frac{k^{1/2}}{N}}\right)^{-1} \quad . \tag{6.44}$$

This relation is consistent with the asymptotic linear behavior near the upper and lower boundaries, as well as with (6.42) if stratification limits the length scale. In the absence of stratification, it predicts a parabolic variation of the length scale. Concluding, we note that the modeled TKE budget (6.41) and model for the length scale in (6.44) form a closed set of equations that is useful for describing simple stratified shear flows.

6.4.3 Consistency with the log law

In the previous chapter it was shown that the log layer is characterized by (a) a layer with constant stress u_*^2, (b) a linear increase of the length scale $l = \kappa z$, and a logarithmic velocity profile as in (6.32). In the following, we want to check under what condition the modeled TKE budget in (6.41) is consistent with this behavior.

We start from the observation that in the log-layer the down-gradient law in (6.2) can be written as $u_*^2 = \nu_t S$. From (6.32), however, we know that $S = u_*/(\kappa z)$ such that $\nu_t = u_*\kappa z$. This can be used to show that the shear production defined in (6.36) becomes

$$P = \frac{u_*^3}{\kappa z} \quad . \tag{6.45}$$

Further, inserting the log-layer expressions $l = \kappa z$ and $\nu_t = u_*\kappa z$ into (6.37), it can be shown that $u_* = c_l k^{1/2}$. Since u_* is constant in the log layer, this implies that also k is constant.

Under these conditions, (6.41) can be greatly simplified. First, the rate term vanishes because the flow is stationary. Second, the transport term (second term on the right hand side) can be ignored because we do not expect any transport of TKE if k is constant. Taking additionally into account that the flow is unstratified, (6.41) reduces to

$$\frac{u_*^3}{\kappa z} = c_\mu \frac{k^{3/2}}{l} = \frac{c_\mu}{c_l^3}\frac{u_*^3}{\kappa z} \tag{6.46}$$

where we have used (6.45) for the shear production on the left hand side, and, in the second step on the right hand, the log layer relations $l = \kappa z$ and $u_* = c_l k^{1/2}$.

We finally conclude that the modeled TKE budget is indeed consistent with the log region of the law of the wall, provided the model parameters obey the relation $c_\mu = c_l^3$.

Appendix A

Basic mathematical tools

When describing physical properties of a fluid, different classes of quantities are appropriate. Some properties, for example temperature, pressure, and energy do not exhibit directional information, and can be fully specified by a single real number. Mathematically, such quantities are described by *scalars*. However, for other variables, for example velocities, forces, and stresses, directional information is essential. These quantities are described by *tensors*. Before examining different ways to work with scalars and tensors, we briefly review the representation of vectors in Cartesian coordinates and provide a mathematical definition of Cartesian tensors.

A.1 Scalar and tensorial quantities

Following the picture of classical mechanics, the kinematics of a moving and deforming fluid is described in the three-dimensional Euclidian space, E_3. The fixed base vectors of the orthonormal base spanning this space are denoted by $\boldsymbol{e}_1$, $\boldsymbol{e}_2$, and $\boldsymbol{e}_3$, and the corresponding coordinates are x_1, x_2, and x_3 (or sometimes also x, y, z). The position vector, $\boldsymbol{x}$, of a point in E_3 can be written as

$$\boldsymbol{x} = x_1\boldsymbol{e}_1 + x_2\boldsymbol{e}_2 + x_3\boldsymbol{e}_3 = \sum_{i=1}^{3} x_i\boldsymbol{e}_i \quad . \tag{A.1}$$

The notation of expressions like (A.1) is considerably simplified by use of the *Einstein summation convention*. According to this convention, the symbol for the sum appearing in (A.1) can be omitted, and the vector $\boldsymbol{x}$ can more compactly be written as

$$\boldsymbol{x} = x_i\boldsymbol{e}_i \quad \text{(summation convention)} \, , \tag{A.2}$$

implying that summation takes place over repeated indices. The summation convention will be used throughout this text.

A property of the space E_3 is that the *dot product* of two (not necessarily orthogonal) unit vectors is defined as the cosine of the angle between these

vectors. It follows that the dot product of two orthogonal unit vectors can be expressed as

$$\boldsymbol{e}_i \cdot \boldsymbol{e}_j = \delta_{ij} \ , \tag{A.3}$$

where δ_{ij} is the *Kronecker delta*. Since the dot product of parallel unit vectors is unity, whereas for orthogonal unit vectors it is zero, the Kronecker delta is defined by

$$\delta_{ij} = \begin{cases} 1 \ , & \text{if } i = j \\ 0 \ , & \text{if } i \neq j \end{cases} \ . \tag{A.4}$$

The component, u_i, of an arbitrary vector, $\boldsymbol{u}$, in the direction of the base vector, $\boldsymbol{e}_i$, can be obtained from the dot product

$$\boldsymbol{u} \cdot \boldsymbol{e}_i = (u_j \boldsymbol{e}_j) \cdot \boldsymbol{e}_i = u_j \delta_{ij} = u_i \ , \tag{A.5}$$

where the summation convention and the properties of the Kronecker delta have been used. The dot product in (A.5) can also be though of as the projection of $\boldsymbol{u}$ in the direction of $\boldsymbol{e}_i$.

A.1.1 Coordinate transformations

As we will see below, the definition of tensors is given in terms of their transformation properties in different coordinates systems. Therefore, it is instructive to consider, in addition to the coordinate system E with base vectors $\boldsymbol{e}_1$, $\boldsymbol{e}_2$, and $\boldsymbol{e}_3$, another Cartesian coordinate system, $\overline{E}$, with base vectors $\overline{\boldsymbol{e}}_1$, $\overline{\boldsymbol{e}}_2$, and $\overline{\boldsymbol{e}}_3$. The system $\overline{E}$ is obtained from E by a number of rotations and reflections of axes; an example is shown in Figure A.1.

As any other vector, the base vectors $\boldsymbol{e}_i$ can be expressed as a linear combination of the base vectors $\overline{\boldsymbol{e}}_j$ according to

$$\boldsymbol{e}_i = a_{ik} \overline{\boldsymbol{e}}_k \ , \tag{A.6}$$

where the components a_{ij} follow from the dot product of (A.6) with $\overline{e}_j$,

$$a_{ij} = \boldsymbol{e}_i \cdot \overline{\boldsymbol{e}}_j \quad . \tag{A.7}$$

The a_{ij} are the *direction cosines*: a_{ij} is the cosine of the angle between the i-axis in the E system and the j-axis in the $\overline{E}$ system. An important property of the direction cosines follows from the dot product of (A.6) with $\boldsymbol{e}_j$,

$$\begin{array}{rcl} \boldsymbol{e}_i \cdot \boldsymbol{e}_j & = & a_{ik} \, \overline{\boldsymbol{e}}_k \cdot \boldsymbol{e}_j \\ \Rightarrow \quad \delta_{ij} & = & a_{ik} a_{jk} \quad . \end{array} \tag{A.8}$$

Similarly, it can be shown that the inverse transformation law for the base vectors is

$$\overline{\boldsymbol{e}}_i = a_{ki} \boldsymbol{e}_k \ , \tag{A.9}$$

and, from scalar multiplication of this equation with $\overline{\boldsymbol{e}}_j$, that

$$\begin{array}{rcl} \overline{\boldsymbol{e}}_i \cdot \overline{\boldsymbol{e}}_j & = & a_{ki} \, \boldsymbol{e}_k \cdot \overline{\boldsymbol{e}}_j \\ \Rightarrow \quad \delta_{ij} & = & a_{ki} a_{kj} \quad . \end{array} \tag{A.10}$$

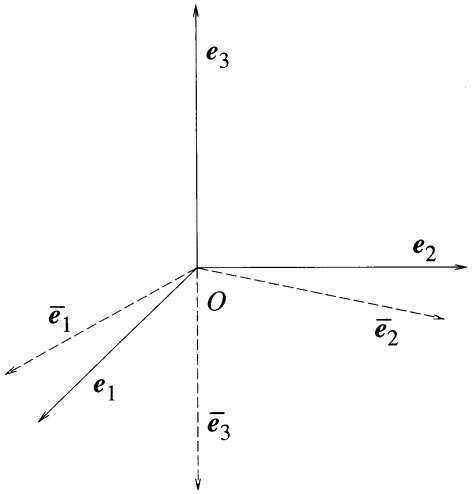

Figure A.1: A sketch of the E (solid lines) and $\overline{E}$ (dashed lines) coordinate systems. In this particular example, $\overline{E}$ is obtained from E by a reflection of the $\overline{\boldsymbol{e}}_3$ axis, and a rotation in the $\boldsymbol{e}_1$-$\boldsymbol{e}_2$ plane.

The position vector, $\boldsymbol{x}$, is the same in both coordinate systems, but its components are different:

$$\boldsymbol{x} = x_i \boldsymbol{e}_i = \overline{x}_j \overline{\boldsymbol{e}}_j \quad . \tag{A.11}$$

The transformation rules for the components are obtained by taking the dot product of this equation with $\boldsymbol{e}_k$ and $\overline{\boldsymbol{e}}_k$:

$$\begin{aligned} x_k &= a_{kj} \overline{x}_j \\ \overline{x}_k &= a_{jk} x_j \quad . \end{aligned} \tag{A.12}$$

A.1.2 The definition of Cartesian tensors

We have seen in the context of (A.11) that a key requirement for a vector is that it is identical in all Cartesian coordinate systems. In other words, the length and direction of a vector should not depend on the choice of the coordinate system. Evidently, this concept should also apply for more general directional quantities called *Cartesian tensors*, which we define in the following.

A *zeroth-order tensor* is a scalar. It has $3^0 = 1$ component, which has the same value in all coordinate systems.

A *first-order tensor* is a vector,

$$\boldsymbol{u} = u_i \boldsymbol{e}_i = \overline{u}_j \overline{\boldsymbol{e}}_j \quad . \tag{A.13}$$

It has $3^1 = 3$ components, transforming according to

$$\overline{u}_j = a_{ij} u_i \ , \tag{A.14}$$

and thus insuring that the vector is the same in all Cartesian coordinate systems. A special case of (A.14) is the position vector defined in (A.11).

A *second-order tensor*,

$$\boldsymbol{T} = T_{ij}\boldsymbol{e}_i \otimes \boldsymbol{e}_j = \overline{T}_{kl}\overline{\boldsymbol{e}}_k \otimes \overline{\boldsymbol{e}}_l \ , \tag{A.15}$$

has $3^2 = 9$ components, by definition transforming according to

$$\overline{T}_{ij} = a_{ki}a_{lj}T_{kl} \quad . \tag{A.16}$$

The symbol $\otimes$ introduced in (A.15) represents the *tensor product* and has no equivalent in standard vector notation. Note that some authors simply write $\boldsymbol{e}_i\boldsymbol{e}_j$ to denote the tensor product $\boldsymbol{e}_i \otimes \boldsymbol{e}_j$.

The transformation rule (A.16) guarantees that the tensor $\boldsymbol{T}$ is always the same, irrespective of the particular Cartesian coordinate system used to represent its components. Transformation rules for tensors of arbitrary order can be constructed by a straightforward extension of (A.16). A Cartesian tensor of order N has 3^N components.

A.1.3 Tensor products

In contrast to scalar multiplications, there are a number of different ways to multiply tensorial quantities. The dot product, for example, has already been introduced above. Using the properties of the dot product of two orthonormal base vectors, (A.3), the dot product of two arbitrary vectors, $\boldsymbol{u}$ and $\boldsymbol{v}$, can be written as

$$\boldsymbol{u} \cdot \boldsymbol{v} = (u_i\boldsymbol{e}_i) \cdot (v_j\boldsymbol{e}_j) = u_iv_j\delta_{ij} = u_iv_i \quad . \tag{A.17}$$

The so-called *inner product* in E_3 is defined by the implicit relations

$$(\boldsymbol{u} \otimes \boldsymbol{v}) \cdot \boldsymbol{w} = (\boldsymbol{v} \cdot \boldsymbol{w})\boldsymbol{u} \tag{A.18}$$

and

$$\boldsymbol{u} \cdot (\boldsymbol{v} \otimes \boldsymbol{w}) = (\boldsymbol{u} \cdot \boldsymbol{v})\boldsymbol{w}. \tag{A.19}$$

This rule can for example be used to evaluate the component form of the inner product of a second-order tensor, $\boldsymbol{A}$, and a vector, $\boldsymbol{b}$, resulting in

$$\begin{aligned} \boldsymbol{A} \cdot \boldsymbol{b} &= (A_{ij}\boldsymbol{e}_i \otimes \boldsymbol{e}_j) \cdot (b_k\boldsymbol{e}_k) = A_{ij}b_k(\boldsymbol{e}_i \otimes \boldsymbol{e}_j) \cdot \boldsymbol{e}_k \\ &= A_{ij}b_k(\boldsymbol{e}_j \cdot \boldsymbol{e}_k)\boldsymbol{e}_i = A_{ij}b_k\delta_{jk}\boldsymbol{e}_i \qquad . \\ &= A_{ij}b_j\boldsymbol{e}_i \end{aligned} \tag{A.20}$$

Some authors write $\boldsymbol{Ab}$ rather than $\boldsymbol{A}\cdot\boldsymbol{b}$ for the product of a tensor and a vector. One can also define the left handed multiplication, $\boldsymbol{b} \cdot \boldsymbol{A}$, which, analogously to the derivation of (A.20), can be shown to correspond to the component form

$$\boldsymbol{b} \cdot \boldsymbol{A} = A_{ij}b_i\boldsymbol{e}_j = A_{ji}b_j\boldsymbol{e}_i \ , \tag{A.21}$$

where in the last step, the dummy indices have been interchanged.

The *cross product* of two (not necessarily orthogonal) unit vectors $\boldsymbol{g}_1$ and $\boldsymbol{g}_2$ is defined as the vector with the length of the sine of the angle α between the two vectors, and the direction orthogonal to the plane which is spanned by $\boldsymbol{g}_1$ and $\boldsymbol{g}_2$, forming a right-hand system. The cross product of two arbitrary vectors, $\boldsymbol{u}$ and $\boldsymbol{v}$, is given by

$$\boldsymbol{r} = \boldsymbol{u} \times \boldsymbol{v} = u_i v_j \boldsymbol{e}_i \times \boldsymbol{e}_j \ , \tag{A.22}$$

where, because of the orthonormality of the base vectors, $\boldsymbol{e}_i$, the definition of the cross product yields

$$\boldsymbol{e}_i \times \boldsymbol{e}_j = \epsilon_{ijk} \boldsymbol{e}_k \ , \tag{A.23}$$

with the so-called *alternating symbol* defined by

$$\varepsilon_{ijk} = \begin{cases} 1 \ , & \text{if } (i,j,k) \text{ cyclic} \\ -1 \ , & \text{if } (i,j,k) \text{ anticyclic} \\ 0 \ , & \text{otherwise} \end{cases} \tag{A.24}$$

Thus, the components of the cross product in (A.22) can compactly be expressed as

$$r_k = \varepsilon_{ijk} u_i v_j \quad . \tag{A.25}$$

Two relations involving the alternating symbol and the Kronecker delta are frequently used. The first is usually called the ε-δ identity,

$$\varepsilon_{ijk} \varepsilon_{ilm} = \delta_{jl} \delta_{km} - \delta_{jm} \delta_{kl} \ , \tag{A.26}$$

the second,

$$\varepsilon_{ijk} \varepsilon_{ijl} = 2 \delta_{kl} \ , \tag{A.27}$$

has not been assigned a particular name. Both identities can be proven by expanding the corresponding expressions.

A.1.4 Symmetric and skew-symmetric tensors

The *transpose* of second-order tensor, $\boldsymbol{T} = T_{ij} \boldsymbol{e}_i \otimes \boldsymbol{e}_j$, is defined by

$$\boldsymbol{T}^T = T_{ji} \boldsymbol{e}_i \otimes \boldsymbol{e}_j = T_{ij} \boldsymbol{e}_j \otimes \boldsymbol{e}_i \quad \text{(transpose)} \quad . \tag{A.28}$$

If the tensor $\boldsymbol{T}$ and its transpose coincide, $\boldsymbol{T} = \boldsymbol{T}^T$, the tensor is said to be *symmetric*. In contrast to that, if the relation $\boldsymbol{T} = -\boldsymbol{T}^T$ holds, the tensor is called *anti-symmetric* or *skew-symmetric*. In indical notation, these statements read

$$\begin{array}{rcll} T_{ij} & = & T_{ji} & \text{(symmetric tensor)} \ , \\ T_{ij} & = & -T_{ji} & \text{(skew-symmetric tensor)} \quad . \end{array} \tag{A.29}$$

Evidently, the diagonal elements of any skew-symmetric tensor are zero, $T_{11} = T_{22} = T_{33} = 0$.

Every second-order tensor can be written as the sum of its symmetric part,

$$T_{(ij)} = \frac{1}{2}(T_{ij} + T_{ji}) \ , \tag{A.30}$$

and skew-symmetric part,

$$T_{[ij]} = \frac{1}{2}(T_{ij} - T_{ji}) \ , \tag{A.31}$$

since the simple relation

$$T_{ij} = T_{(ij)} + T_{[ij]} \tag{A.32}$$

is valid for any second-order tensor.

A.2 Derivatives

A.2.1 Ordinary and partial derivatives

For a one-dimensional, sufficiently smooth function, $f(x)$, the *ordinary derivative* is defined by

$$\frac{\mathrm{d}}{\mathrm{d}x} f(x) = \lim_{\Delta x \to 0} \frac{f(x + \Delta x) - f(x)}{\Delta x} \quad . \tag{A.33}$$

For a vector-valued function of a vector, $\boldsymbol{x} = (x_1, x_2, \ldots, x_n)$, the *partial derivative* with respect to the coordinate x_i is defined by

$$\frac{\partial}{\partial x_i} f(x_1, \ldots, x_n) = \lim_{\Delta x \to 0} \frac{f(x_1, \ldots, x_i + \Delta x, \ldots, x_n) - f(x_1, \ldots, x_n)}{\Delta x} \quad . \tag{A.34}$$

A.2.2 The Nabla-operator

When working with tensorial quantities in E_3, a number of generalised derivatives, playing an important role in fluid mechanics, can be introduced. Generalised derivatives are most conveniently written in symbolic form using the so-called *Nabla-operator*, for an orthonormal basis defined by

$$\nabla = \frac{\partial}{\partial x_i} \boldsymbol{e}_i \quad . \tag{A.35}$$

Using this convention, the *gradient* of a tensorial quantity, $\boldsymbol{\phi}$ is defined by

$$\nabla \boldsymbol{\phi} = \nabla \otimes \boldsymbol{\phi} = \left(\frac{\partial}{\partial x_k} \boldsymbol{e}_k \right) \otimes \boldsymbol{\phi} \quad . \tag{A.36}$$

For example, if $\boldsymbol{\phi} = \boldsymbol{u}(\boldsymbol{x})$ is a vector, then its gradient is the second-order tensor given by

$$\nabla \boldsymbol{u} = \left(\frac{\partial}{\partial x_k} \boldsymbol{e}_k \right) \otimes (u_i \boldsymbol{e}_i) = \frac{\partial u_i}{\partial x_k} \boldsymbol{e}_k \otimes \boldsymbol{e}_i \quad . \tag{A.37}$$

If $\boldsymbol{\phi}$ is a tensor of order N, then its gradient is a tensor of order $N+1$. For example, if $\phi = c$ corresponds to a zeroth-order tensor (scalar), the gradient is a first-order tensor (vector):

$$\nabla c = \left(\frac{\partial}{\partial x_i}\boldsymbol{e}_i\right) c = \frac{\partial c}{\partial x_i}\boldsymbol{e}_i \quad . \tag{A.38}$$

Note that the dyadic product in (A.36) degenerates into a standard multiplication in this case.

Similarly, the *divergence* of a tensorial quantity, $\boldsymbol{\phi}$, is defined by

$$\nabla \cdot \boldsymbol{\phi} = \left(\frac{\partial}{\partial x_k}\boldsymbol{e}_k\right) \cdot \boldsymbol{\phi} \quad . \tag{A.39}$$

Taking the second-order tensor $\boldsymbol{T}$ as an example, the divergence of $\boldsymbol{T}$ corresponds to the vector

$$\begin{aligned} \nabla \cdot \boldsymbol{T} &= \left(\frac{\partial}{\partial x_k}\boldsymbol{e}_k\right) \cdot (T_{ij}\boldsymbol{e}_i \otimes \boldsymbol{e}_j) = \frac{\partial T_{ij}}{\partial x_k}\delta_{ki}\boldsymbol{e}_j \\ &= \frac{\partial T_{ij}}{\partial x_i}\boldsymbol{e}_j = \frac{\partial T_{ji}}{\partial x_j}\boldsymbol{e}_i \quad . \end{aligned} \tag{A.40}$$

Note that in some texts the divergence in (A.40) is obtained by summing over the second index, instead over the first. If $\boldsymbol{\phi}$ is a tensor of order N, then its divergence is a tensor of order $N-1$.

The *curl* of a tensorial quantity is evaluated from the cross-product with the Nabla-operator. Evaluated for a vector field, $\boldsymbol{u}(\boldsymbol{x})$, this procedure yields the vector

$$\nabla \times \boldsymbol{u} = \varepsilon_{ijk}\frac{\partial u_k}{\partial x_j}\boldsymbol{e}_i \quad . \tag{A.41}$$

Finally, the *Laplacian* results from the application of the scalar product of two Nabla-operators, operating on a scalar field, ϕ. The result of this operation is

$$\nabla \cdot \nabla\phi = \nabla^2\phi = \left(\frac{\partial}{\partial x_i}\boldsymbol{e}_i\right) \cdot \left(\frac{\partial \phi}{\partial x_j}\boldsymbol{e}_j\right) = \frac{\partial}{\partial x_i}\left(\frac{\partial \phi}{\partial x_j}\right)\delta_{ij} = \frac{\partial^2 \phi}{\partial x_i^2} \ , \tag{A.42}$$

thus yielding a scalar expression.

Using the above-mentioned vector identities in connection with the Nabla-operator, a number of additional relations can be obtained. The cross product of the curl of a vector with itself for example yields

$$(\nabla \times \boldsymbol{u}) \times \boldsymbol{u} = \boldsymbol{u} \cdot \nabla\boldsymbol{u} - \frac{1}{2}\nabla(\boldsymbol{u} \cdot \boldsymbol{u}) \quad . \tag{A.43}$$

To proof this relation, we introduce the abbreviation $\boldsymbol{a} = \nabla \times \boldsymbol{u}$ in (A.43),

leading to

$$\begin{aligned}
(\nabla \times \boldsymbol{u}) \times \boldsymbol{u} &= \boldsymbol{a} \times \boldsymbol{u} \\
&= \varepsilon_{ijk} a_j u_k \boldsymbol{e}_i \\
&= \varepsilon_{ijk} \varepsilon_{jlm} \frac{\partial u_m}{\partial x_l} u_k \boldsymbol{e}_i \\
&= (\delta_{kl}\delta_{im} - \delta_{km}\delta_{il}) \frac{\partial u_m}{\partial x_l} u_k \boldsymbol{e}_i \\
&= \left(\frac{\partial u_i}{\partial x_k} u_k - \frac{\partial u_k}{\partial x_i} u_k \right) \boldsymbol{e}_i \\
&= \left(u_k \frac{\partial u_i}{\partial x_k} - \frac{1}{2} \frac{\partial (u_k u_k)}{\partial x_i} \right) \boldsymbol{e}_i \ ,
\end{aligned}$$

which corresponds to (A.43).

In a similar way, a number of other well-known relatations between the vectors $\boldsymbol{a}$ and $\boldsymbol{b}$ and the scalars c and d can be derived. For these quantities, the following identities, useful in later chapters, can be shown to hold:

$$\nabla \times \nabla c = \boldsymbol{0} \ , \tag{A.44}$$

$$(d \nabla c) \times \nabla c = \boldsymbol{0} \ , \tag{A.45}$$

$$\nabla \cdot (\nabla \times \boldsymbol{a}) = 0, \tag{A.46}$$

$$\boldsymbol{a} \cdot \nabla \boldsymbol{a} = (\nabla \times \boldsymbol{a}) \times \boldsymbol{a} + \frac{1}{2} \nabla (\boldsymbol{a} \cdot \boldsymbol{a}) \ , \tag{A.47}$$

$$\nabla \times \nabla^2 \boldsymbol{a} = \nabla^2 (\nabla \times \boldsymbol{a}) \ , \tag{A.48}$$

$$\nabla \times (\boldsymbol{a} \times \boldsymbol{b}) = \boldsymbol{a} (\nabla \cdot \boldsymbol{b}) + (\boldsymbol{b} \cdot \nabla) \boldsymbol{a} - \boldsymbol{b} (\nabla \cdot \boldsymbol{a}) - (\boldsymbol{a} \cdot \nabla) \boldsymbol{b} \quad . \tag{A.49}$$

A.3 Statistical description of random variables

We have seen in Chapter 1 that due the chaotic character of the solutions of the Navier-Stokes equations at high Reynolds numbers, instantaneous flow quantities behave like random variables. This implies, for example, that repeating an identical experiment many times will lead to different, unpredictable values of the instantaneous velocity $u(\boldsymbol{x}, t)$ at a given point in space and time. Nevertheless, in a statistical sense, it may still be possible to describe the behavior of $u(\boldsymbol{x}, t)$. To this end, the basic concepts of required for the statistical description of turbulence are summarized in the following.

A.3.1 Probability

The *probability* that u is smaller, for example, than a given upper threshold V_u is written as

$$p = P\{u < V_u\} \,, \tag{A.50}$$

where, for the moment, it is sufficient to use the intuitive understanding that p is a real number ($0 \leq p \leq 1$) signifying the likelyhood of the occurence of this event. For an impossible event p is zero, and for a sure event it is unity.

A.3.2 The cumulative distribution function

The probability of any event of the type (A.50) can be inferred from the *cumulative distribution function* (CDF) defined as

$$F(V) = P\{u < V\} \,, \tag{A.51}$$

where we have introduced the so-called *sample space variable* V corresponding to u. We have $F(V) \geq 0$ everywhere, where $F(V)$ is a monotonically increasing function with the properties $F(-\infty) = 0$ and $F(\infty) = 1$. For given $F(V)$ the probability that u is located in a given range between V_l and V_u is easily evaluated as

$$F(V_u) - F(V_l) = P\{V_l \leq u \leq V_u\} \quad . \tag{A.52}$$

A.3.3 The probability density function

The *probability density function* (PDF) follows from the CDF as:

$$f(V) \equiv \frac{\mathrm{d}F(V)}{\mathrm{d}V} \quad . \tag{A.53}$$

Using the properties of $F(V)$ it is easy to show that the PDF is non-negative ($f(V) \geq 0$), and that it satisfies the normalization condition

$$\int_{-\infty}^{\infty} f(V)\mathrm{d}V = 1 \,, \tag{A.54}$$

with $f(-\infty) = f(\infty) = 0$. The PDF characterizes the probablity of u to be in the infinitesimally small range between V and $V + \mathrm{d}V$. It should be noted that the PDF (or equally the CDF) fully characterizes any random variable u.

A.3.4 Means and moments

The *mean* or *expected value* of the random variable u is defined as the first moment of the PDF,

$$\langle u \rangle = \int_{-\infty}^{\infty} V f(V)\mathrm{d}V \quad . \tag{A.55}$$

The (random) fluctuations of involved in u then follow from the simple relation

$$u' = u - \langle u \rangle \quad . \tag{A.56}$$

From these definitions, using the properties of the PDF discussed above, it is easy to show (see assignments) that the mean satisfies the following relations

- $\langle a \rangle = a$,
- $\langle au \rangle = a\langle u \rangle$,
- $\langle \langle u \rangle \rangle = \langle u \rangle$,
- $\langle u' \rangle = 0$,

where a is a constant and u the random variable.

The variance of u is then defined as the second moment of the fluctuations,

$$\mathrm{var}(u) \equiv \left\langle u'^2 \right\rangle = \int_{-\infty}^{\infty} (V - \langle u \rangle)^2 f(V) \mathrm{d}V \quad . \tag{A.57}$$

The square root of the variance is called the *standard deviation*: $\mathrm{std}(u) \equiv \sqrt{\mathrm{var}(u)}$.

A.4 Isotropic tensor functions

As dicussed in Chapter 5, statistical expressions simplify considerably under isotropic conditions. In isotropic turbulence, by definition, no preferred spatial directions exist such that, for example, all turbulent fluxes have to vanish (as a flux always implies a direction).

It turns out that also functional relationships between tensorial quantities adopt particularly simple forms in isotropic turbulence. Let's consider a simple example in which a second-order tensor $\boldsymbol{R}$ depends on an arbitrary vector $\boldsymbol{r}$:

$$\boldsymbol{R} = \hat{\boldsymbol{R}}(\boldsymbol{r}) \quad . \tag{A.58}$$

You may think of this as a relation between the correlation tensor $\boldsymbol{R}$ and the separation vector $\boldsymbol{r}$ connecting two points in space (both quantities were introduced in Chapter 5).

Now consider a second-order tensor $\boldsymbol{Q}$ that has the property $\boldsymbol{Q}\boldsymbol{Q}^T = \boldsymbol{I}$, or, in index notation: $Q_{ij}Q_{lj} = \delta_{il}$. It is known from linear algebra that for such tensors the operation

$$\boldsymbol{r}^* = \boldsymbol{Q}\boldsymbol{r} \ , \tag{A.59}$$

corresponds to a pure rotation of $\boldsymbol{r}$ that does not change its length. Similarly, also the tensor $\boldsymbol{R}$ can be rotated but, because of the double base vectors of second-order tensors, two tensor multiplications with $\boldsymbol{Q}$ are required:

$$\boldsymbol{R}^* = \boldsymbol{Q}\boldsymbol{R}\boldsymbol{Q}^T \quad . \tag{A.60}$$

The condition of isotropy can now easily be constructed from the following argument. If all statistical fields are assumed to be isotropic, i.e. if the statistics has no preferred directions, the functional relationship between the original quantities $\boldsymbol{R}$ and $\boldsymbol{r}$ has to be exactly identical to that between the rotated quantities:

$$\boldsymbol{R}^* = \hat{\boldsymbol{R}}(\boldsymbol{r}^*) \;, \tag{A.61}$$

where it is essential to note that $\hat{\boldsymbol{R}}$ remains unchanged compared to (A.58). Using (A.59) and (A.60), the condition in (A.61) can be reformulated as

$$\boldsymbol{Q}\boldsymbol{R}\boldsymbol{Q}^T = \hat{\boldsymbol{R}}(\boldsymbol{Q}\boldsymbol{r}) \quad . \tag{A.62}$$

A small branch of mathematics called *tensor represenation theory* considers isotropy conditions like that in (A.62), and tries to derive explicit functional relationships that satisfy them. For example, it can be shown that the most general function satisfying (A.62) is of the form

$$\boldsymbol{R} = A(r)\boldsymbol{I} + B(r)\boldsymbol{r} \otimes \boldsymbol{r} \;, \tag{A.63}$$

where A and B are two unknown functions of $r = |\boldsymbol{r}|$. In index notation, (A.63) becomes

$$R_{ij} = A(r)\delta_{ij} + B(r)r_i r_j \quad . \tag{A.64}$$

These relations will be frequently used in Chapter 5 to simplify functional relationships in isotropic turbulence.

Bibliography

Kolmogorov, A. N., 1941: Local structure of turbulence in incompressible viscous fluid of very large Reynolds number. *Doklady Akademiya Nauk SSSR*, **30**, 299–301.

Kundu, P. K. and I. M. Cohen, 2008: *Fluid Mechanics*. 4th ed., Academic Press, London, UK, 872 pp.

Pope, S. B., 2000: *Turbulent Flows*. Cambridge University Press, Cambridge, UK, 806 pp.